



**NAVAL
POSTGRADUATE
SCHOOL**

MONTEREY, CALIFORNIA

THESIS

**COOPERATIVE CONTROL OF DISTRIBUTED
AUTONOMOUS SYSTEMS WITH APPLICATIONS
TO WIRELESS SENSOR NETWORKS**

by

Mark G. Richard

June 2009

Thesis Co-Advisors:

Deok Jin Lee
Isaac I. Kaminer

Approved for public release; distribution is unlimited

THIS PAGE INTENTIONALLY LEFT BLANK

REPORT DOCUMENTATION PAGE			<i>Form Approved OMB No. 0704-0188</i>
Public reporting burden for this collection of information is estimated to average 1 hour per response, including the time for reviewing instruction, searching existing data sources, gathering and maintaining the data needed, and completing and reviewing the collection of information. Send comments regarding this burden estimate or any other aspect of this collection of information, including suggestions for reducing this burden, to Washington headquarters Services, Directorate for Information Operations and Reports, 1215 Jefferson Davis Highway, Suite 1204, Arlington, VA 22202-4302, and to the Office of Management and Budget, Paperwork Reduction Project (0704-0188) Washington DC 20503.			
1. AGENCY USE ONLY (Leave blank)	2. REPORT DATE June 2009	3. REPORT TYPE AND DATES COVERED Master's Thesis	
4. TITLE AND SUBTITLE Cooperative Control of Distributed Autonomous Systems with Applications to Wireless Sensor Networks		5. FUNDING NUMBERS	
6. AUTHOR(S) Mark G. Richard		8. PERFORMING ORGANIZATION REPORT NUMBER	
7. PERFORMING ORGANIZATION NAME(S) AND ADDRESS(ES) Naval Postgraduate School Monterey, CA 93943-5000		10. SPONSORING/MONITORING AGENCY REPORT NUMBER	
9. SPONSORING /MONITORING AGENCY NAME(S) AND ADDRESS(ES) N/A		11. SUPPLEMENTARY NOTES The views expressed in this thesis are those of the author and do not reflect the official policy or position of the Department of Defense or the U.S. Government.	
12a. DISTRIBUTION / AVAILABILITY STATEMENT Approved for public release; distribution is unlimited		12b. DISTRIBUTION CODE	
13. ABSTRACT (maximum 200 words) This thesis extends previously developed self-tuning adaptive control algorithms to be applied to a scenario where multiple vehicles autonomously form a communication chain which maximizes the bandwidth of a wireless sensor network. In the simulated scenario, multiple unmanned aerial vehicles are guided to positions that optimize communication links between multiple ground antennas. Guidance is provided by a self-tuning extremum controller, which uses adaptive techniques to autonomously guide a vehicle to the optimal location with respect to a cost function in an uncertain and noisy environment. In the case of high-bandwidth communication, this optimal location is the point where signal-to-noise ratio is maximized between two antennas. Using UAVs as relay nodes, an optimized communication chain allows for greater communication range and bandwidth across a network. Control system models are developed and tested using computer and hardware-in-the-loop simulations, which will be validated with a flight test at a future date.			
14. SUBJECT TERMS Unmanned Aerial Vehicle, UAV, Extremum Seeking, Simulink, High Bandwidth Communication Links, SNR Model, Coordinated Control, Cooperative control, Decentralized Control, Wireless Sensor Network		15. NUMBER OF PAGES 68	
		16. PRICE CODE	
17. SECURITY CLASSIFICATION OF REPORT Unclassified	18. SECURITY CLASSIFICATION OF THIS PAGE Unclassified	19. SECURITY CLASSIFICATION OF ABSTRACT Unclassified	20. LIMITATION OF ABSTRACT UU

THIS PAGE INTENTIONALLY LEFT BLANK

Approved for public release; distribution in unlimited

**COOPERATIVE CONTROL OF DISTRIBUTED AUTONOMOUS SYSTEMS
WITH APPLICATIONS TO WIRELESS SENSOR NETWORKS**

Mark G. Richard
Ensign, United States Navy
B.S., United States Naval Academy, 2008

Submitted in partial fulfillment of the
requirements for the degree of

MASTER OF SCIENCE IN MECHANICAL ENGINEERING

from the

**NAVAL POSTGRADUATE SCHOOL
June 2009**

Author: Mark G. Richard

Approved by: Dr. Deok Jin Lee
Co-Advisor

Isaac I. Kaminer
Co-Advisor

Knox T. Millsaps, Chairman
Department of Mechanical and Astronautical Engineering

THIS PAGE INTENTIONALLY LEFT BLANK

ABSTRACT

This thesis extends previously developed self-tuning adaptive control algorithms to be applied to a scenario where multiple vehicles autonomously form a communication chain which maximizes the bandwidth of a wireless sensor network. In the simulated scenario, multiple unmanned aerial vehicles are guided to positions that optimize communication links between multiple ground antennas. Guidance is provided by a self-tuning extremum controller, which uses adaptive techniques to autonomously guide a vehicle to the optimal location with respect to a cost function in an uncertain and noisy environment. In the case of high-bandwidth communication, this optimal location is the point where signal-to-noise ratio is maximized between two antennas. Using UAVs as relay nodes, an optimized communication chain allows for greater communication range and bandwidth across a network. Control system models are developed and tested using computer and hardware-in-the-loop simulations, which will be validated with a flight test at a future date.

THIS PAGE INTENTIONALLY LEFT BLANK

TABLE OF CONTENTS

I.	INTRODUCTION.....	1
A.	MOTIVATION	1
B.	TACTICAL NETWORK TOPOLOGY (TNT) PROGRAM.....	1
C.	THESIS OBJECTIVES.....	1
II.	BACKGROUND	3
A.	WIRELESS COMMUNICATION NETWORKS	3
B.	MODELING COMMUNICATION NETWORKS	4
1.	Free-space Radiowave Transmission	5
2.	Antenna Pattern Losses.....	6
C.	CONTROL FOR HIGH BANDWIDTH COMMUNICATION.....	6
1.	Extremum Seeking Gradient Estimation.....	7
2.	Signal to Noise Ratio Estimation	9
III.	PREVIOUS WORK.....	11
A.	UAV DYNAMIC MODEL	11
B.	SNR MODEL	11
1.	Path Loss Model.....	12
2.	Antenna Pattern Loss Model	12
C.	SELF-TUNING EXTREMUM CONTROLLER.....	14
1.	Gradient Ascent	14
2.	Convergence	16
3.	SNR Cost Function	16
D.	INITIAL FLIGHT TEST.....	17
E.	MULTIPLE GROUND NODE SIMULATION.....	19
IV.	DECENTRALIZED EXTREMUM CONTROL OF MULTIPLE UAVS	23
A.	DISTRIBUTED CONTROL OF AUTONOMOUS SYSTEMS.....	23
B.	DISTRIBUTED EXTREMUM CONTROL FLIGHT SETUP	25
1.	Distributed Cost Function for Multiple UAV Control.....	27
2.	SNR Modeling of Link Between UAVs.....	27
C.	INITIAL GUIDANCE	28
1.	Virtual Node Guidance.....	29
2.	Direct Artificial Potential Guidance.....	30
D.	DECENTRALIZED EXTRUMUM CONTROL FOR TWO UAVS.....	32
1.	Convergence Control.....	32
E.	LOITERING FORMATION CONTROL.....	32
1.	Optimal Loitering Formation	32
2.	Synchronization Method 1 – Logic Controller.....	34
3.	Synchronization Method 2 – Phase Controller	36
F.	MULTIPLE UAV SIMULATION	38
V.	FUTURE APPLICATIONS.....	41
A.	MULTIPLE UAV RELAY TO MULTIPLE NODES.....	41

B.	TARGET TRACKING AND SURVEILLANCE	43
VI.	CONCLUSIONS AND FUTURE WORK.....	45
A.	CONCLUSIONS	45
B.	FUTURE WORK.....	45
APPENDIX:	SIMULINK DIAGRAMS.....	47
A.	ORBIT CENTER ERROR CALCULATION SCRIPT	49
	LIST OF REFERENCES.....	51
	INITIAL DISTRIBUTION LIST	53

LIST OF FIGURES

Figure 1.	Gain Pattern for 2.2 dB Omni Directional Antenna. From [2].	6
Figure 2.	Extremum Seeking Control Architecture. From [1]	8
Figure 3.	SNR map of 2 Ground Antennas. From [2].	10
Figure 4.	Single Node 2-D SNR Distribution. From [2].	10
Figure 5.	Line-of Sight Path Loss Vector. From [2].	13
Figure 6.	Bank Angle Effect. From [2].	13
Figure 7.	Extremum Controller Convergence. From [9].	15
Figure 8.	UAV Flight Trajectory. From [2].	18
Figure 9.	SNR for Link with Ground Station 1. From [2].	18
Figure 10.	SNR of Link with Ground Station 2. From [2].	19
Figure 11.	Multiple Ground Node Link Structure.	19
Figure 12.	Multiple Node Simulated UAV Trajectory with SNR Estimates	20
Figure 13.	Multiple Node Simulated SNR Values	20
Figure 14.	Distributed Control Architecture. From [3].	23
Figure 15.	Multiple UAV Link Structure	25
Figure 16.	Distributed Control Architecture	26
Figure 17.	Distributed Cost Function for 2 UAV Communication Chain	27
Figure 18.	Decentralized Extremum Control Schematic. From [1].	28
Figure 19.	Virtual Node Guidance Link Structure	29
Figure 20.	SNR Map for UAV1 with Links to Ground Node 1 and UAV 2	31
Figure 21.	SNR Potential Function Along Straight Path Between Nodes	31
Figure 22.	Formation Synchronization Parameters	33
Figure 23.	SNR of Phase Spacing Configurations for Loitering Formation	33
Figure 24.	Synchronization Flight Path of Follower Aircraft	34
Figure 25.	Follower Flight Path with Phase Feedback Control	37
Figure 26.	Control Mode Flowchart.	38
Figure 27.	Multiple UAV Simulated Flight Trajectory with SNR Estimates	39
Figure 28.	SNR Values for Multiple UAV Simulation	40
Figure 29.	Vehicle Trajectory for 2 UAV and 4 Ground Node Simulation	42
Figure 30.	SNR Values for 2 UAV and 4 Ground Node Simulation	42
Figure 31.	Vehicle Trajectory for Extremum Target Tracking Simulation	44
Figure 32.	NPS Soaring Glider. From [2].	45
Figure 33.	Multiple UAV Simulation Block Diagram	47
Figure 34.	Stateflow Control Mode Switching Logic	48
Figure 35.	Phase Synchronization Controller	48
Figure 36.	Phase Synchronization Phase and Orbit Center Error Calculations	49

THIS PAGE INTENTIONALLY LEFT BLANK

LIST OF TABLES

Table 1. Simulation Parameters38

ACKNOWLEDGMENTS

First, I would like to thank my advisor Professor Deok Jin Lee for his patience and advice throughout the course of this project. Professor Lee's positive attitude and dedication gave me motivation to push through setbacks, of which there were many. I would also like to thank advisor Professor Isaac Kaminer for allowing me to work on this project. Additionally, I would like to thank Professor Kevin Jones, Professor Vadimir Dobrokhodov, Klas Andersson, and Jeff Wurz for their assistance on this project.

THIS PAGE INTENTIONALLY LEFT BLANK

I. INTRODUCTION

A. MOTIVATION

Wireless networking for high bandwidth communication currently has applications such as surveillance, wide-area sensing, environmental monitoring, search and rescue, and communication relay. Algorithms that optimize a network using teams of distributed robots are an emerging technology and a popular area of research. The challenge of controlling multiple vehicles falls on implementing these algorithms in real-time using distributed autonomous control.

This thesis extends previously developed, self-tuning, adaptive control algorithms to be applied to a scenario where multiple vehicles autonomously form a communication chain that maximizes the bandwidth of a wireless sensor network. In a simulated scenario, multiple unmanned aerial vehicles are guided to positions that optimize the communication links between multiple ground antennas. The advantage of using UAVs as distributed relay nodes include extended range, greater coverage area, and eliminating any line-of-sight requirement for communication between nodes.

B. TACTICAL NETWORK TOPOLOGY (TNT) PROGRAM

The TNT program is an exercise supported by the United States Special Operations Command (USSOCOM) and hosted by NPS quarterly at Camp Roberts, CA. The goal of this program is to explore viable applications of emerging technologies related to communications, vehicle control, and ad-hoc wireless mesh networks. Recent TNT flight tests from NPS Center for Autonomous Vehicle Research have focused on target identification and tracking, path following, and high-bandwidth communications. Flight tests are conducted at the Center of Interdisciplinary Remotely-Piloted Aircraft Studies (CIRPAS) facility located at McMillan Air Field in Camp Roberts, CA.

C. THESIS OBJECTIVES

At the NPS Center for autonomous vehicle Research, flight tests have been conducted using a single UAV as a relay node between two ground stations. The goal of

this thesis is to extend previously developed adaptive algorithms to be applied to a scenario where multiple UAVs autonomously form a communication chain optimizing the bandwidth of a wireless sensor network. Additional simulations are conducted to explore new applications of decentralized control related to high bandwidth communication and surveillance.

II. BACKGROUND

A. WIRELESS COMMUNICATION NETWORKS

A network consists of series of communication devices, such as computers, cellular phones, or portable radios that are able to send and receive messages. For local area networks these devices must either be hardwired to the network or communicate via a router connected to the network. This setup can only be used if the devices are in close proximity to wireless routers or are directly connected to the network through cables. New developments in the last decade have led to the development of wireless mesh networks. In a mesh network each node is able to communicate to every other node, and does not rely on a single source as in a local area network [7]. The network maintains signal strength by using a series of hops to transfer information, increasing the bandwidth of the network with each additional node. Thus, the total coverage area created by a wireless mesh network can potentially be as large as an entire city with enough devices [8]. In a mesh network, information can be easily re-routed to account for nodes that are added or removed, which creates robustness to node failure [6]. Wireless mesh networks use IEEE 802.11 a, b, and c wireless protocols, which are compatible with most wireless devices in use today.

A wireless sensor network consists of a series of sensor devices that are able to send and receive data with the other nodes via a wireless mesh network. Wireless sensor networks have become popular in oceanography and environmental survey fields because they allow a team of vehicles to autonomously collect data over a large area [6]. In the military, wireless sensor networks are used for surveillance and communication relay. The robustness to loss of a single node in wireless sensor network allows for a team of mobile sensors to continue a mission even if several sensors are lost [8].

An Ad-hoc wireless mesh network consists of several mobile wireless devices with links that automatically adjust for the motion of the nodes [7]. With each node able to communicate with every other node, an ad-hoc network can find the most efficient

path to route a message. In an intelligent ad-hoc network the nodes can reposition themselves autonomously in a configuration that optimizes the network for a desired mission.

B. MODELING COMMUNICATION NETWORKS

The link quality between two radio antennas can be affected by received signal power, sensor specifications and environmental factors [2]. For a receiving antenna to be able to detect and demodulate an incoming signal, the received power must be greater than the receiver's sensitivity. If the received signal power is not greater than this minimum threshold value, link breakage could result [2]. The Link margin relates received signal strength and the minimum receiver threshold [2]

$$\text{Link Margin} = P_r - R_{sens} \quad (2.1)$$

where P_r is the received power and R_{sens} is the minimum received signal that will guarantee reliable operation in dB.

The link between antennas also depends on the noise level of system devices and environment. The desired position of an antenna is a location where the received signal is maximized and noise is minimized. Received signal power and noise power are related by the signal-to-noise ratio (SNR) [2].

$$SNR = \frac{\text{Received Signal Power}}{\text{Noise Power}} \quad (2.2)$$

The total throughput of a communication link will be optimal when its channel capacity is maximized. The Shannon-Hartley theorem relates channel capacity (C, bits per second) to bandwidth (W, Hz) and SNR [2].

$$C = W \log_2(1 + SNR) \quad (2.3)$$

Since SNR and channel capacity are directly proportional, the channel capacity of a link will be maximized when SNR is at its peak value.

1. Free-space Radiowave Transmission

The received power, P_r , of an antenna for line-of-sight communication can be determined by the Friis free space transmission Equation [2].

$$P_r = \frac{P_t G_t G_r \lambda^2}{(4\pi)^2 D^2} \quad (2.4)$$

where P_t is the transmitted power, G_t is the transmitter gain, G_r is the receiver gain, λ is the wavelength in meters, and D is the separation distance between transmitter and receiver in meters. This equation computes the free space path loss between two antennas with no obstructions in the path between them. The antenna gain represents antenna directivity and efficiency, while the inverse distance square of separation distance accounts for the spherical wave front spreading [9]. Expressed in dB, the transmission equation becomes [2].

$$P_r = P_t + G_t + G_r - L_{path} \quad (2.5)$$

with line-of-sight path loss is represented by [2]

$$L_{path} [dB] = P_r - P_t = 32.4 + 20 \log(f) [MHz] + 20 \log(d) [km] \quad (2.6)$$

where f is the signal frequency in MHz and d is the separation distance in km.

From the Friis transmission equation, the SNR of the receiver can be determined [2].

$$SNR [dB] = P_r - NL \quad (2.7)$$

where NL is the system noise level in dB.

2. Antenna Pattern Losses

In addition to the line-of-sight path loss, losses also result from the orientation of the antennas relative to each other. In a spherical coordinate system, the radiation pattern of an antenna is determined by measuring the electric field intensity of a sphere at a fixed radius [2]. The electric field intensity is represented by the antenna gain, which will vary with elevation and position about the antenna's azimuth depending on the polarization and specifications of the antenna. Attenuation due to antenna gain patterns can be accounted for in the free-space equation by determining the orientation of the sending and receiving antennas with respect to each other. The free space equation becomes [2]

$$P_r [dB] = P_t + G_t + G_r - L_{path} - L_{AP} \quad (2.8)$$

with the term L_{AP} accounting for the gain pattern losses. Figure 1 illustrates the gain pattern for a 2.2 dB omni-directional antenna, which can be attached to a small UAV.

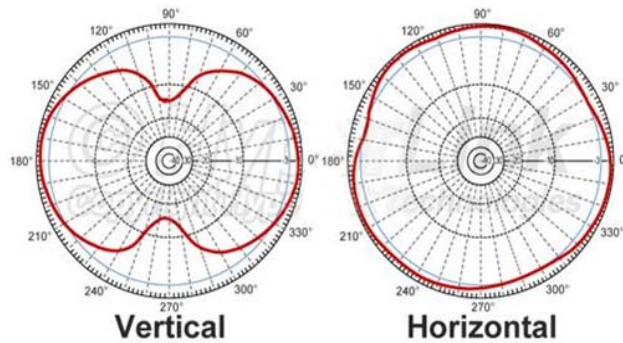


Figure 1. Gain Pattern for 2.2 dB Omni Directional Antenna. From [2].

C. CONTROL FOR HIGH BANDWIDTH COMMUNICATION

In adaptive control, the goal is to drive the set point of a dynamic system to an optimal one by finding the extremum, a local maximum or minimum, of an objective function [4]. For optimal communication, a network of vehicles can autonomously position themselves to maximize link quality by finding the extremum of an SNR cost

function. Numerical gradient descent techniques can be used to find this extremum provided that the cost function is defined mathematically. However, for an unknown and noisy environment, it is not possible to mathematically model SNR with a continuous cost function [1]. Additionally, numerical gradient estimation can be computationally intensive and difficult to implement in real time. The control algorithm used in this thesis combines an extremum seeking gradient estimation scheme with a traditional gradient ascent controller [1]. The advantages of this controller are that it does not require a model of the objective function and avoids costly Jacobian and Hessian matrix calculations in the gradient estimation step [8]. The simplicity of this controller makes it ideal for use with a network of vehicles that do not have a large amount of onboard computational power.

1. Extremum Seeking Gradient Estimation

Extremum Seeking control has been researched since the 1950s and has proved to be a useful and efficient adaptive control method. In the 1990s, extremum seeking saw resurgence as researchers found it particularly useful for real time optimization [4]. In 2000, Krstic and Wang provided stability proofs for extremum control, which led to its widespread use in adaptive control applications such as formation flight, bioreactor operation, engine mapping, and beam matching in particle accelerators [4]. Extremum seeking can be particularly useful for nonlinear systems with a local minimum or maximum with respect to which the system can be optimized [8]. The most common extremum seeking method involves perturbation, or injecting a sinusoidal signal into the plant to generate a gradient estimate. An extremum seeking flow chart is shown in Figure 2.

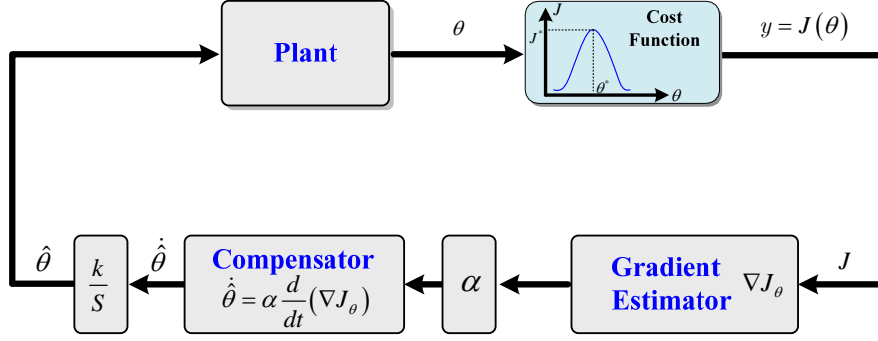


Figure 2. Extremum Seeking Control Architecture. From [1]

For an adjustable parameter $\psi \in \mathbb{R}$, the output of the plant, $y \in \mathbb{R}$, is defined as [1]

$$y = J(\psi) \quad (2.9)$$

where $J(\psi)$ is a performance function with an extremum value at $\psi = \psi^*$. To estimate the gradient of the objective function, a sinusoidal signal is injected into the plant to perturb $J(\psi)$ about its current heading value $\hat{\psi}$. The output of the plant becomes [1]

$$y = J(\hat{\psi} + a \sin \omega t) \approx J(\hat{\psi}) + a \left. \frac{\partial J}{\partial \psi} \right|_{\psi=\hat{\psi}} \sin \omega t \quad (2.10)$$

after applying a high pass filter, $\frac{s}{s+h}$, the DC offset, $J(\hat{\psi})$, is eliminated and the plant output signal becomes [1]

$$y_{HP} = a \left. \frac{\partial J}{\partial \psi} \right|_{\psi=\hat{\psi}} \sin \omega t \quad (2.11)$$

Injecting a second sinusoidal signal demodulates the y_{hp} into a high and low frequency components [1]

$$\zeta = \frac{1}{2} a \left. \frac{\partial J}{\partial \psi} \right|_{\psi=\hat{\psi}} - \frac{1}{2} a \left. \frac{\partial J}{\partial \psi} \right|_{\psi=\hat{\psi}} \cos 2\omega t \quad (2.12)$$

applying a low pass filter, $\frac{l}{s+l}$, gives the gradient estimate [1]

$$y_{LP} = \frac{1}{2} a \left. \frac{\partial J}{\partial \psi} \right|_{\psi=\hat{\psi}} \quad (2.13)$$

Assuming the objective function is quadratic in nature, the cost is defined as [1]

$$J(\psi) = J(\psi^*) + \frac{1}{2} J''(\psi^*) (\hat{\psi} - \psi^*)^2 \quad (2.14)$$

where the gradient about $\hat{\psi}$ is [1]

$$\nabla J_{\hat{\psi}} = \left. \frac{\partial J}{\partial \psi} \right|_{\psi=\hat{\psi}} \approx J''(\psi - \psi^*) \quad (2.15)$$

This gradient estimate can be used by a steepest ascent controller to guide a vehicle to the peak of an objective function. Extremum seeking gradient estimation is advantageous for real time applications where complex gradient calculations are not feasible. Additionally, an extremum seeking gradient estimator does not require a continuous objective function model, which makes it ideal for unknown and noisy environments.

2. Signal to Noise Ratio Estimation

In an uncertain and cluttered environment, actual SNR measurements obtained from sensors are noisy and have a low sample rate (1 Hz). To improve these sensor measurements, the SNR cost function can be modeled using an artificial potential field of the predicted SNR [2]. If the locations of the ground antennas are known, the SNR of each link can be modeled with the free space transmission equations to create a continuous SNR map. Although this model does not account for effects of scattering, reflection, refraction and extraneous environmental noise, it provides a reasonable estimate to compare to actual SNR measurements [2]. Additionally the scale of the SNR potential field allows the user to accurately tune the extremum seeking parameters of the controller to guarantee stability.

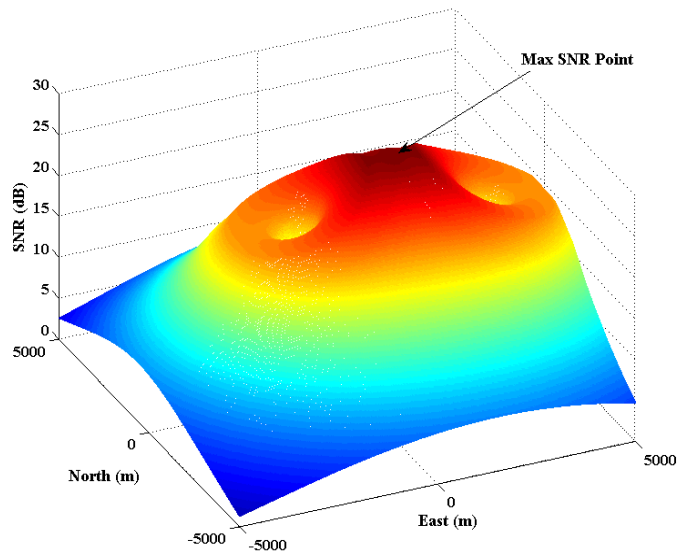


Figure 3. SNR map of 2 Ground Antennas. From [2].

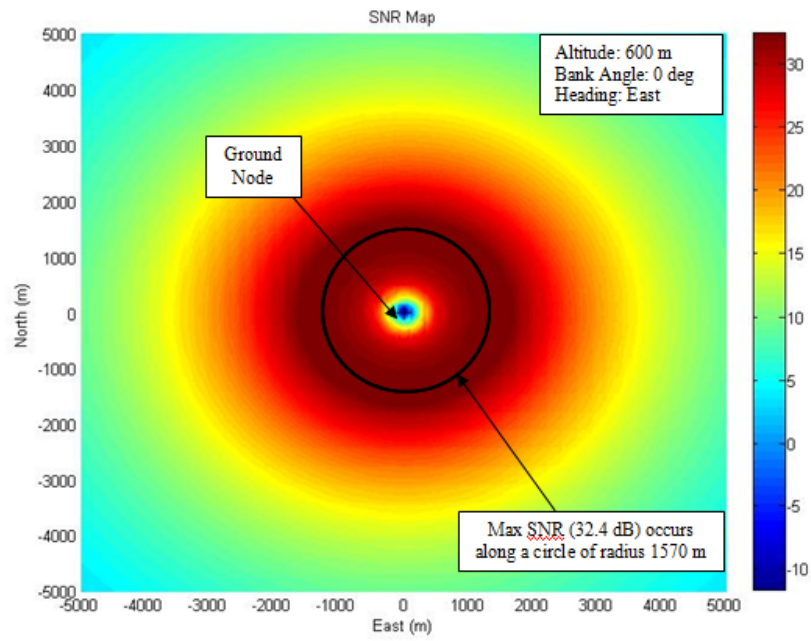


Figure 4. Single Node 2-D SNR Distribution. From [2].

III. PREVIOUS WORK

MATLAB Simulink 6.5 by Mathworks is used to develop and test self-tuning extremum control algorithms. Additionally, the Aerospace blockset by Aerosim and Stateflow visual coding software by Mathworks are incorporated into the Simulink block diagrams.

A. UAV DYNAMIC MODEL

To simulate the dynamics of a small aircraft, a 6 degree of freedom vehicle model from the Aerosim blockset was incorporated into a closed loop Simulink model. The inputs to the model are commanded velocity, bank angle, and altitude. The control input is bank angle with constant altitude and velocity commands. Using an approximation of bank angle dynamics, the commanded bank angle is determined from heading rate output of the extremum controller [2].

$$\phi = \tan^{-1} \left(\frac{V \dot{\psi}_{cmd}}{g} \right) \quad (3.1)$$

where V is the forward velocity of the vehicle, $\dot{\psi}_{cmd}$ is the commanded heading rate, and g is acceleration due to gravity. The outputs of the dynamic model are heading, roll angle, and position in a local tangent plane coordinate frame.

B. SNR MODEL

In [2], a model was developed to determine the SNR of a link between a ground node and UAV by calculating the path and antenna pattern losses. The input variables to the model are the UAV flight trajectory and the location of the ground node, both in local tangent plane coordinates. The output of the model is the SNR of the link, which is the input for the extremum seeking gradient estimation algorithm [2].

1. Path Loss Model

Equation 2.8 develops the calculation of SNR between a ground node and a UAV using the Friis free space transmission equation.

$$SNR_{Path} [dB] = P_t + G_t + G_r - L_{Path} - NL$$

$$L_{Path} = 32.4 + 20 \log(f) [MHz] + 20 \log(d(t)) [km]$$

f = frequency (2400 MHz)

$$d(t) = \sqrt{(x(t) - x_{node})^2 + (y(t) - y_{node})^2 + (z(t) - z_{node})^2} [km]$$

P_t = transmitter power (28 dBm)

G_t = transmitter antenna gain (9 dB)

G_r = receiver antenna gain (3 dB)

NL = system noise level (-95 dBm)

The specified gains and noise level are characteristic of the data sheets for the actual antennas used to create communication links during flight tests.

2. Antenna Pattern Loss Model

The antenna pattern loss for the link between ground antenna and UAV can be modeled using the antenna gain patterns provided from the antenna manufacturers. To determine antenna pattern loss, the incident angle for each antenna must be calculated using ray tracing.

$$P_{uav,LTP} = \begin{bmatrix} x(t) \\ y(t) \\ z(t) \end{bmatrix} \quad \text{and} \quad P_{node,LTP} = \begin{bmatrix} x_{node} \\ y_{node} \\ z_{node} \end{bmatrix} \quad (3.2)$$

the incident angle is defined as

$$\theta(t) = \tan^{-1} \left(\frac{(z(t) - z_{node})}{\sqrt{(x(t) - x_{node})^2 + (y(t) - y_{node})^2}} \right) \quad (3.3)$$

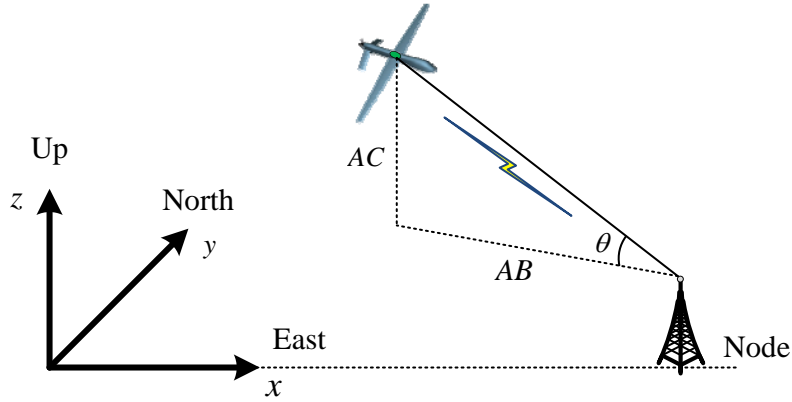


Figure 5. Line-of Sight Path Loss Vector. From [2].

The banking motion of the UAV affects the angle of the onboard antenna and introduces noise to the total SNR measurement. The bank angle has the effect of decreasing or increasing the angle of arrival depending on its heading with respect to the ground node. SNR will be most sensitive to bank angle when the UAV travels on a path perpendicular to the ground node. Conversely, bank angle will have no effect on SNR when the UAV is flying directly toward or away from the ground node [2].

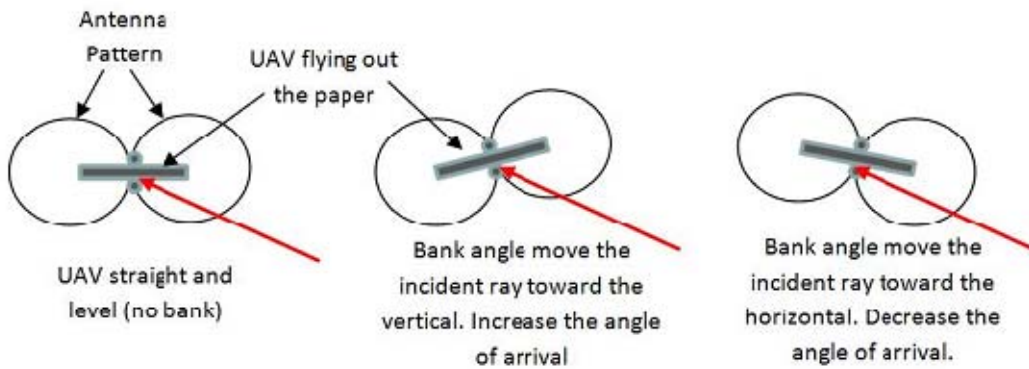


Figure 6. Bank Angle Effect. From [2].

This bank angle effect is modeled using a sine function to determine the influence of bank on the arrival angle based on the UAV's heading [2].

$$\text{Bank Angle Effect} = \phi \cdot \sin(\phi - \psi) \quad (3.4)$$

where ϕ is the UAV roll angle, ϕ is the bearing to the sending antenna, and ψ is UAV heading. The input into the antenna gain pattern chart is the arrival angle, which is the difference between the incident angle and the bank angle [2].

$$\text{Arrival Angle} = -\theta(t) - \text{Bank Angle Effect} \quad (3.5)$$

The antenna pattern loss is then determined from a look-up table modeled after antenna manufacturer data [2].

C. SELF-TUNING EXTREMUM CONTROLLER

1. Gradient Ascent

With heading rate as the control input to the UAV dynamic model, the goal of the controller is to command the UAV to fly in a direction that ascends the gradient of the cost function. Using traditional gradient ascent numerical techniques, the desired heading is determined [1]

$$\psi_{k+1} = \psi_k + \alpha_k \nabla J_\psi \quad (3.6)$$

where α_k is the step length and ∇J_ψ is the gradient obtained using extremum seeking perturbation methods. To obtain the control input of the dynamic model, heading rate equation needs to be differentiated [1]

$$\frac{d\psi(t)}{dt} = \alpha(t) \frac{d}{dt} (\nabla J_\psi) \quad (3.7)$$

If the objective function is assumed to be quadratic, it will be of the form [1]

$$J(\hat{\psi}(t)) = J^* + \frac{\mu}{2} (\hat{\psi}(t) - \psi^*)^2 + w(t) \quad (3.8)$$

The output of the extremum-seeking controller will be the gradient estimate for the current heading [1]

$$\nabla J_{\hat{\psi}(t)} = \frac{\partial J(\hat{\psi}(t))}{\partial \hat{\psi}(t)} = \mu(\hat{\psi}(t) - \psi^*) \quad (3.9)$$

To employ the gradient descent algorithm from Equation 3.7, the gradient estimate needs to be differentiated [1].

$$\frac{\partial}{\partial t}(\nabla J_{\hat{\psi}(t)}) = \mu(\psi(t)) \quad (3.10)$$

Inserting this solution into Equation 3.7 results in a heading rate command for the steepest descent of the cost function [1].

$$\begin{aligned} \dot{\psi}_{com}(t) &= \frac{d\psi(t)}{dt} = \alpha(t) \frac{d}{dt}(\nabla J_{\psi}) \\ &= \mu\alpha(t)\psi(t) \end{aligned} \quad (3.11)$$

Instead of commanding a heading pointing directly at the extremum point, it is more desirable for the UAV to gradually converge to a steady state heading rate value [1].

$$\dot{\psi}_{cmd} = \dot{\psi}_{ss} + \mu\alpha(t)\psi(t) \quad (3.12)$$

This controller will command the UAV to find where the gradient is minimized and circle about that point.

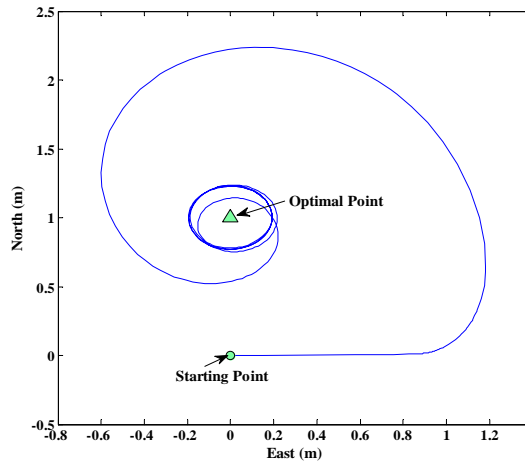


Figure 7. Extremum Controller Convergence. From [9].

2. Convergence

For steepest ascent controller to provide smooth fast convergence, it is necessary to determine an optimal time step scale factor, $\alpha(t)$ [1]. Bounds on this step length value are specified by a set of criteria known as the Armijo-Wolfe conditions. These conditions limit the gradient ascent rate if the step length is too small and command the UAV to fly a straight line if the step length is too large. The value for alpha is chosen such that [1]

$$\Delta J_{k+1} = J_{k+1} - J_k \quad (3.13)$$

$$\alpha_{k+1} = \gamma \cdot \alpha_k, \quad \text{where} \begin{cases} 0 < \gamma < 1, & \text{if } \Delta J_{k+1} > \tau_{th} \\ \gamma \geq 1, & \text{else } \Delta J_{k+1} < \tau_{th} \end{cases} \quad (3.14)$$

3. SNR Cost Function

The object of the self-tuning extremum controller is to command a heading rate that climbs the gradient of an SNR cost function to the desired objective. For a case where the link between a single ground node and UAV is optimized, the cost function will be $J = SNR$, with SNR designated as the figure of merit for the link [1]. In a scenario where multiple communication links are optimized, a distributed cost function must be used. This cost function will combine the SNR values for the links in such a way that the UAV is able to maximize the throughput of the network. It is important to note that the end-to-end throughput of a series of nodes will be limited by the link with the lowest SNR value [2]. Thus the objective of the controller is to drive the SNR of all communication links to the same value. At the optimal point, all links will have the same SNR value, and that SNR will be at a maximum. To force the SNR of all links to the same value, the UAV ascends the gradient of the link with the smallest SNR value.

Using the defined cost function, the extremum controller regulates vehicle states using a search sequence that minimizes the performance output. The extremum control problem is interpreted as [3]

$$\min_{\mathbf{x}_k \in D} J_k(\mathbf{x}_k) \quad \text{subject to } \mathbf{x}_{k+1} = \mathbf{f}(\mathbf{x}_k, \mathbf{u}_k) \quad (3.15)$$

For optimizing the combined SNR of a UAV with links to two ground nodes, the cost function is chosen to be [2]

$$\begin{aligned} J_{total} &= \min(J_1, J_2) \\ &= k \log\left(\frac{1}{J_1} + \frac{1}{J_2}\right) \end{aligned} \quad (3.16)$$

J_1 and J_2 are the SNR value of the communication links with ground tower 1 and 2, respectively and κ is a shaping parameter used to adjust the slope of the gradient close to the gradient peak. The control objective is to find an optimal control input such that the gradient terms between UAVs and communication nodes are nearly zero as shown in Equation 3.17 [3].

$$\text{Find} \left\{ \lim_{u_{uav}(t) \rightarrow \infty} [\nabla J_{1,uav}(t) - \nabla J_{2,uav}(t)] \simeq 0 \right\} \quad (3.17)$$

where $\nabla J_{1,uav}(t)$ is the gradient of the relative SNR signal between the node 1 and the UAV, and $\nabla J_{2,uav}(t)$ is the gradient of the relative SNR signal between the node 2 and the UAV .

D. INITIAL FLIGHT TEST

The flight test in reference [1] used a self-tuning extremum controller to find a theoretical SNR peak between two ground antennas. The extremum controller used a model-based approach to find the location of the anticipated SNR peak. During the flight actual SNR readings were taken and were shown to be within a reasonable range of the SNR model.

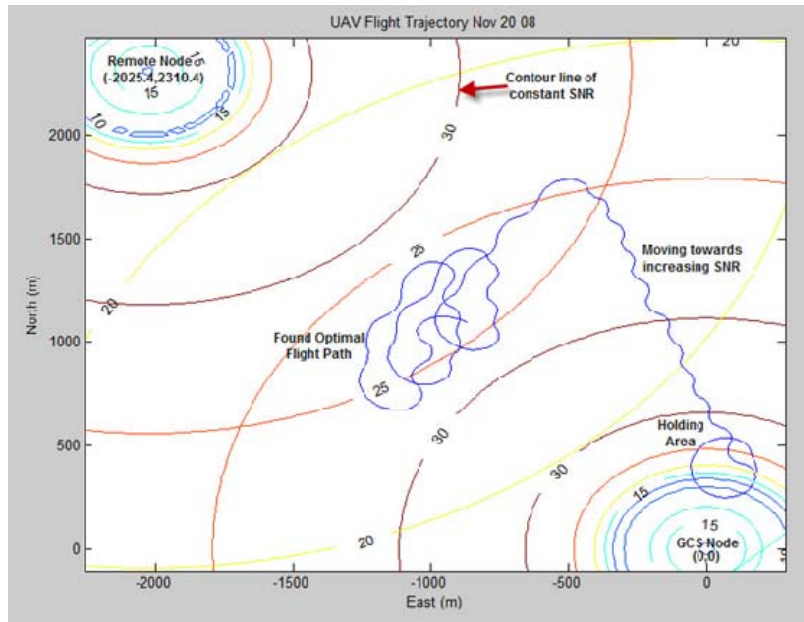


Figure 8. UAV Flight Trajectory. From [2].

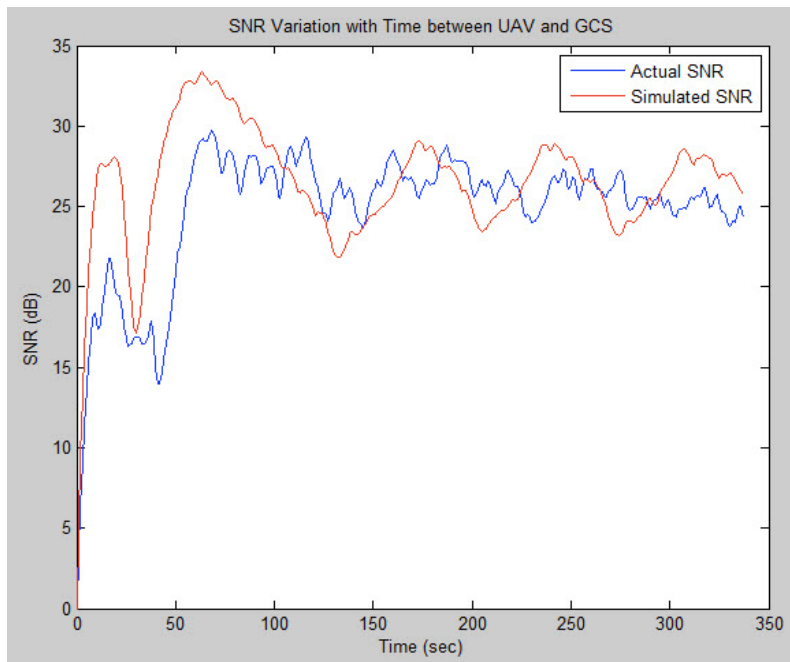


Figure 9. SNR for Link with Ground Station 1. From [2].

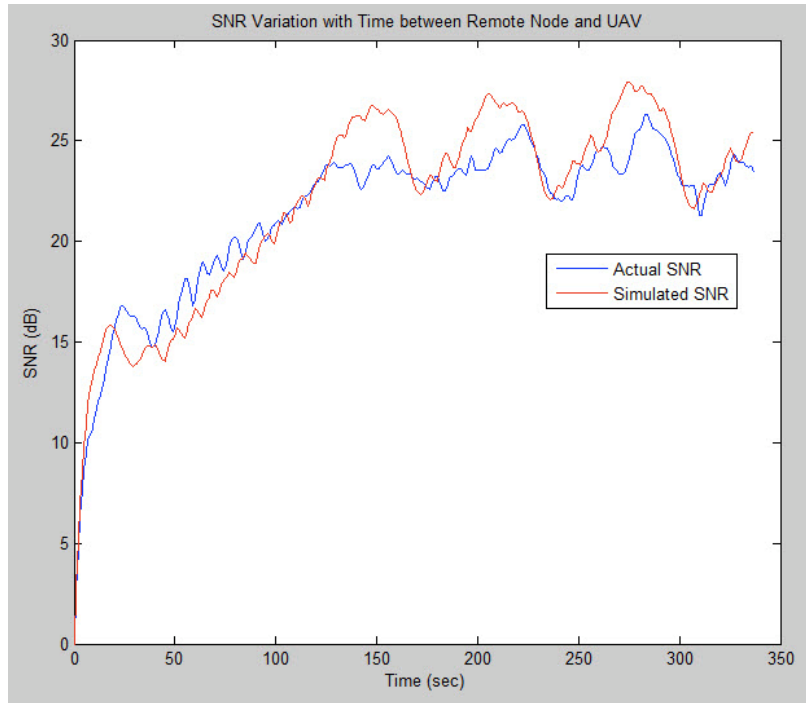


Figure 10. SNR of Link with Ground Station 2. From [2].

E. MULTIPLE GROUND NODE SIMULATION

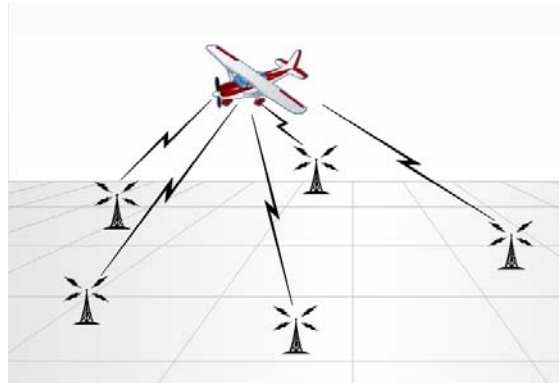


Figure 11. Multiple Ground Node Link Structure

Extending the confirmed flight test case to include many ground nodes does not require any modification of the extremum controller. In the simulated scenario, a single UAV repositions itself to find the optimal communication relay point to five ground antennas. The SNR cost function for this scenario becomes

$$\begin{aligned}
 J_{total} &= \min(J_1, J_2, J_3, J_4, J_5) \\
 &= k \log \left(\frac{1}{J_1} + \frac{1}{J_2} + \frac{1}{J_3} + \frac{1}{J_4} + \frac{1}{J_5} \right)
 \end{aligned}
 \tag{3.16}$$

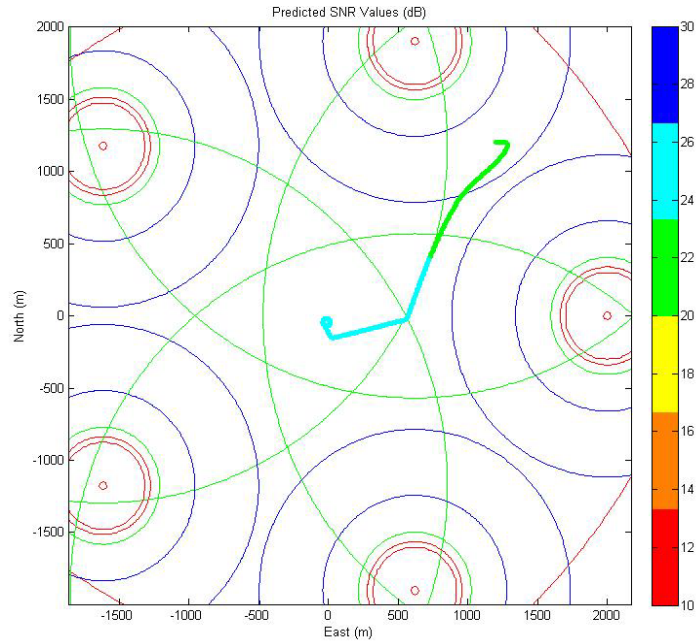


Figure 12. Multiple Node Simulated UAV Trajectory with SNR Estimates

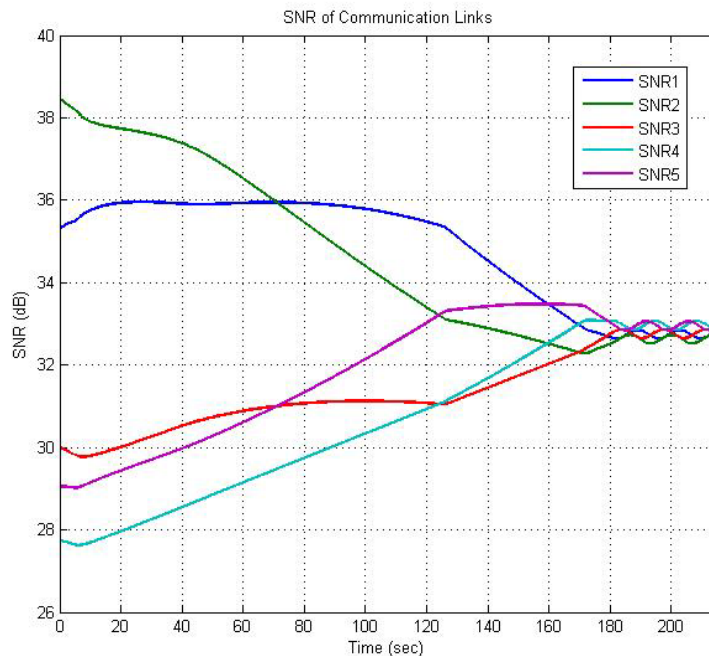


Figure 13. Multiple Node Simulated SNR Values

This simulation demonstrates that a mobile relay node can be used to optimize the SNR of an arbitrary number of received signals. As opposed to extending the end-to-end throughput of a communication chain, the relay node in this scenario optimizes network coverage for a series of spaced out nodes. An application where this setup would be useful is when a series of ground users need to communicate, but have no line-of-sight contact with other users.

THIS PAGE INTENTIONALLY LEFT BLANK

IV. DECENTRALIZED EXTREMUM CONTROL OF MULTIPLE UAVS

A. DISTRIBUTED CONTROL OF AUTONOMOUS SYSTEMS

A distributed system consists of a series of independent subsystems that cooperate to perform a task. Decentralized, or distributed control refers to the manner in which members of a multi-agent system communicate with and react to the dynamics of other members in order to accomplish a specified mission [7]. This command structure occurs in flocks of birds and schools of fish, where independent members collaborate to achieve a common goal by reacting to movements of their neighbors [6]. Centralized control, the opposite of distributed, suggests a single, universal controller responsible for planning and assigning movement for each component of a system. With a distributed control system, autonomous agents are capable of sensing, acting, and communicating such that minimal direction is provided from a centralized command station [8]. Advantages of distributed control include the ability of the group to adapt to unknown and dynamic environments and robustness to fault of a single member [3].

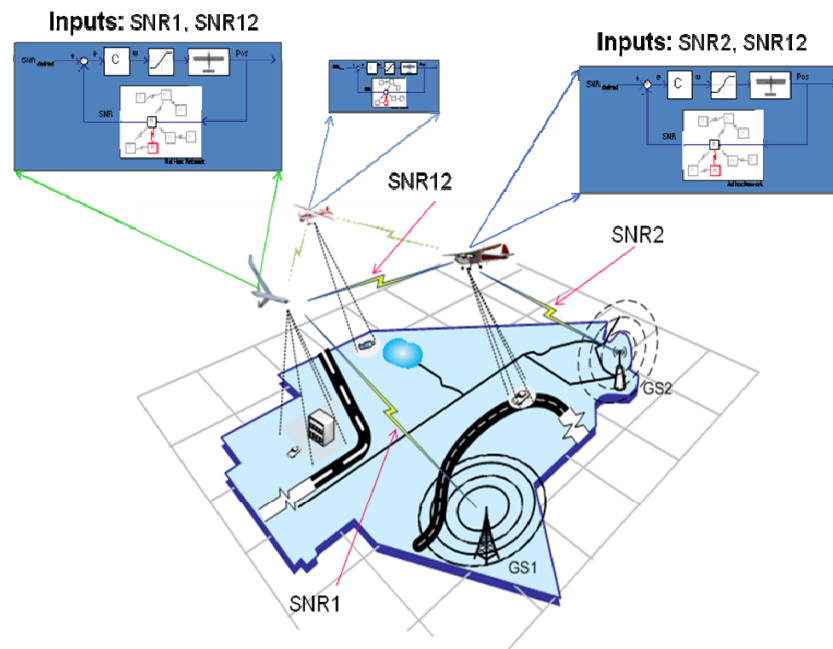


Figure 14. Distributed Control Architecture. From [3].

For decentralized control of multiple UAVs with general N nodes, it is necessary to define relative cost functions between the nodes and UAVs (UAV to ground node and UAV to UAV) for inputs to each extremum controller. Suppose there are two communication nodes (i, j) with two UAVs (l, m) in a linear network such that a node can send data to next neighbor node. Then, two relative cost functions are defined by [3]

$$J_{i,l} = SNR_{i,l}(\mathbf{p}_{i,l}), J_{l,m} = SNR_{l,m}(\mathbf{p}_{l,m}), J_{m,j} = SNR_{m,j}(\mathbf{p}_{m,j}) \quad (3.17)$$

where $J_{i,l}$ is the SNR between the i ground node and UAV l , which is a function of the relative position vector $\mathbf{p}_{i,l}$ between them. Then, the cost function for the l vehicle is calculated by [3]

$$\begin{aligned} J_l &= \min(J_{i,l}, J_{l,m}) \\ &= \kappa_l \log\left(\frac{1}{J_{i,l}} + \frac{1}{J_{l,m}}\right) \end{aligned} \quad (3.18)$$

Similarly, the cost function for the m vehicle is obtained by

$$\begin{aligned} J_m &= \min(J_{l,m}, J_{m,j}) \\ &= \kappa_m \log\left(\frac{1}{J_{l,m}} + \frac{1}{J_{m,j}}\right) \end{aligned} \quad (3.19)$$

The relative cost functions (J_l, J_m) are used as inputs for the extremum controller for each vehicle [3]

$$\lim_{t \rightarrow \infty} [\nabla J_{l,m}(t) - \nabla J_{m,j}(t)] \simeq 0 \quad (3.20)$$

Where $\nabla J_{1,uav}(t)$ is the gradient of the relative SNR signal between the node 1 and the UAV, and $\nabla J_{2,uav}(t)$ is the gradient of the relative SNR signal between the node 2 and the UAV. The control objective is to find optimal control inputs such that the gradient terms between UAVs and communication nodes become equal as shown in Equation (34) [3].

For a mission involving multiple unmanned vehicles, decentralized control implies that each member determines its movement using an onboard controller. This controller typically can react to the position and orientation of other members in addition to onboard sensor measurements. In a wireless sensor network, each vehicle could potentially share sensor information with other members such that the vehicles reposition themselves to perform a mission more efficiently. Although there are varying degrees of decentralized control, the goal is to increase autonomy in a network of vehicles so that coordinated tasks can be performed with minimal user oversight. A decentralized control structure would be particularly useful for optimizing communication in military wireless networks in that users would be able to focus on a mission while allowing autonomous vehicles to maintain a communication network.

B. DISTRIBUTED EXTREMUM CONTROL FLIGHT SETUP

In a scenario where a multiple UAVs collaborate to form a communication chain, decentralized control allows for each vehicle to find the optimal location for communication relay using an onboard self-tuning extremum controller. The UAVs in the communication chain will position themselves in a link structure assigned by the ground control station. In the simulated scenario, two UAVs form a communication chain between two ground nodes by finding the location where the SNR of all links is at the same optimal value. The decentralized link structure of a scenario where two UAVs form a communication chain is shown in **Error! Reference source not found.**

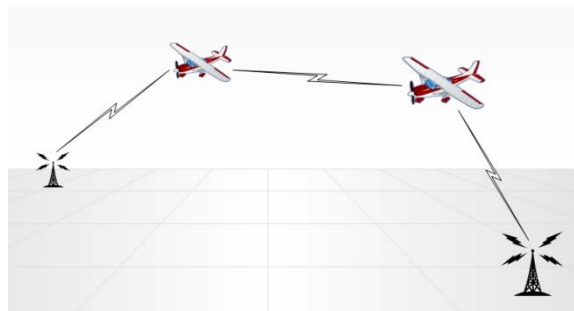


Figure 15. Multiple UAV Link Structure

With sufficient onboard processing power, each UAV would ideally be able to calculate the SNR of each received signal using measurements and relay this information directly to other UAVs. However, for an experimental flight test, the SNR data processing step cannot be conducted onboard using the available hardware. In the flight test configuration, the SNR data of each link is processed at the ground control station and sent back to each UAV where trajectory is determined by an onboard extremum controller. Although this setup requires a greater amount of computation by the ground control station, it simulates a scenario where multiple UAVs are guided using only received SNR data. The control structure of the simulated scenario is shown in **Error! Reference source not found.**

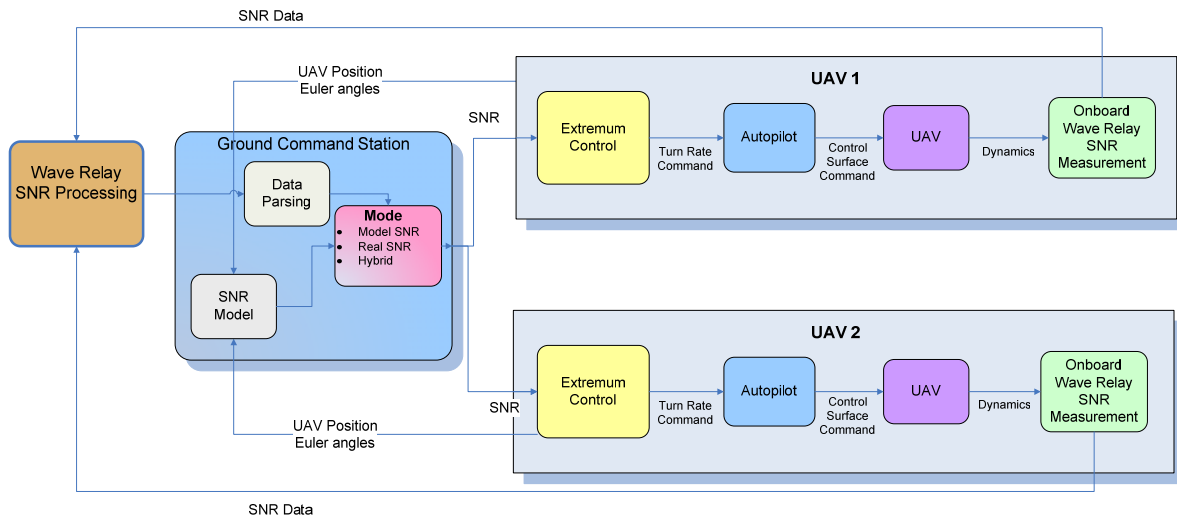


Figure 16. Distributed Control Architecture

The SNR measurements sent from the ground station may either be model based, actual measurements, or a hybrid estimate using a filtered combination of the two. The actual SNR measurements can be used to update the model-based estimates to obtain a more accurate continuous SNR map.

1. Distributed Cost Function for Multiple UAV Control

In the two UAV case, two separate, yet dependent, cost functions are needed to create an optimal communication chain.

UAV 1 Cost Function

$$J_{UAV1} = \min(J_1, J_{12})$$

$$= \kappa \left(\frac{1}{J_1} + \frac{1}{J_{12}} \right)$$

UAV 2 Cost Function

$$J_{UAV2} = \min(J_2, J_{12})$$

$$= \kappa \left(\frac{1}{J_2} + \frac{1}{J_{12}} \right)$$

(4.1)

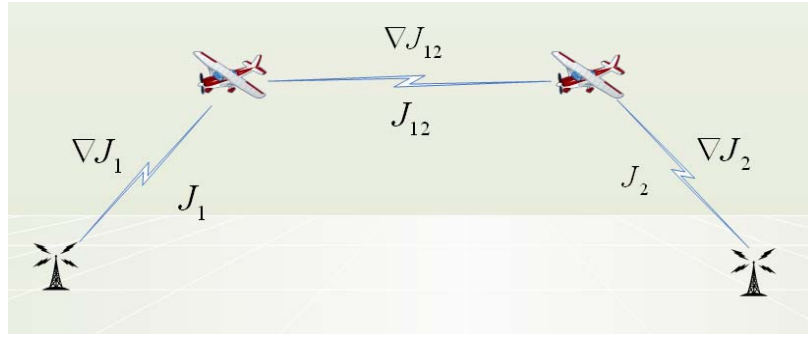


Figure 17. Distributed Cost Function for 2 UAV Communication Chain

The two UAVs climb the gradient toward a final position where $J_1, J_2,$ and J_{12} are driven to an equal SNR and the gradient of each cost function is zero.

2. SNR Modeling of Link Between UAVs

In the original SNR model, all links were modeled to reflect communication between a ground antenna and a UAV. In the multiple UAV case, the SNR model is altered to reflect communication between two UAVs. The antenna gains are decreased to reflect the less powerful antennas onboard the UAVs. Additionally the bank angle effect in the antenna pattern loss is modified to take into account the banking motion of both UAVs.

$$\text{Bank Angle Effect} = (\phi_1 - \phi_2) \sin(\psi_1 - \psi_2)$$

(4.2)

where ϕ is roll angle and ψ is heading in radians.

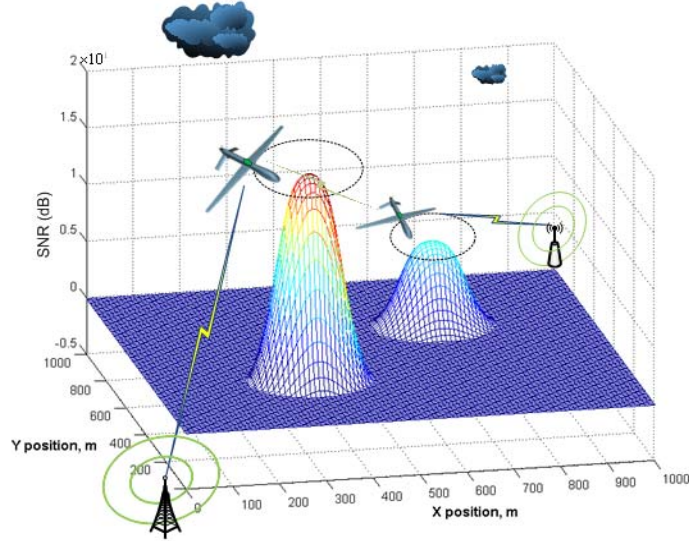


Figure 18. Decentralized Extremum Control Schematic. From [1].

C. INITIAL GUIDANCE

Initial simulations of the decentralized control setup previously described exhibited slow convergence to the final optimal positions when the initial offset distance was large. For distributed SNR optimization using multiple UAVs as relay nodes, the SNR map is dynamic since the vehicles are moving relative to each other. For a dynamic SNR map, the two UAVs will only be able to converge to the gradient peaks when the gradient is slowly changing. Since SNR between the UAVs is mostly a function of separation distance, for convergence the relative distance between the aircraft must slowly change. If the UAVs are initialized far from the optimal point and each other, the gradient ascent algorithm becomes unstable due to the rapidly changing SNR gradient.

To decrease convergence time of the decentralized extremum control scheme, initial guidance is required to position the UAVs relatively close to the optimal communication point. Two decentralized guidance methods were explored to accomplish this task.

1. Virtual Node Guidance

The first method used for initial guidance utilizes an artificial node placed at the midpoint of the two ground antennas. The artificial SNR measurement is calculated using the free-space SNR model between a UAV and ground antenna. This allows for the same extremum controller to be used and simulates a fixed node case.

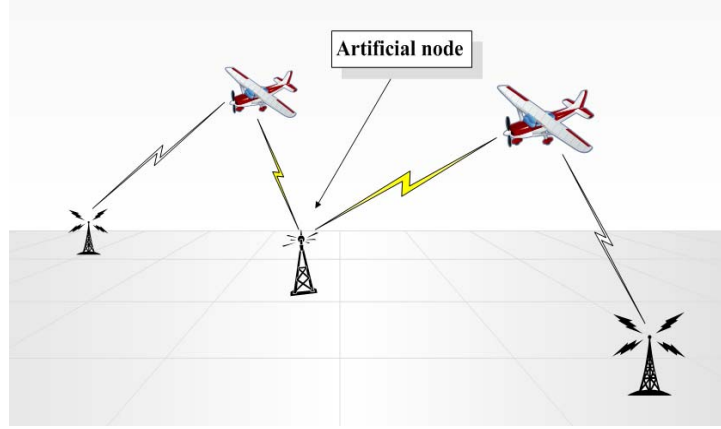


Figure 19. Virtual Node Guidance Link Structure

With this configuration the SNR measurement from each respective ground node could be combined with the artificial SNR using a distributed cost function [1].

$$\begin{aligned}
 J_{UAV1,artificial} &= \min(J_1, J_{artificial1}) & J_{UAV2,artificial} &= \min(J_2, J_{artificial2}) \\
 &= \kappa \left(\frac{1}{J_1} + \frac{1}{J_{artificial1}} \right) & &= \kappa \left(\frac{1}{J_2} + \frac{1}{J_{artificial2}} \right)
 \end{aligned} \tag{4.3}$$

To conduct a completely autonomous mission using extremum control and multiple control modes, the user must design robust switching criteria. Once both UAVs have minimized the gradient of the artificial guidance cost function, guidance is shifted to decentralized extremum control using the link between the UAVs. Convergence for virtual node guidance is defined when [1]

$$\Delta J_{UAV1} = |J_1 - J_{1,artificial}| < 1$$

and $\Delta J_{UAV2} = |J_2 - J_{2,artificial}| < 1$

(4.4)

2. Direct Artificial Potential Guidance

An alternative to the virtual tower approach is to directly specify a single artificial potential function for each UAV along the line connecting the towers. The extremum gradient ascent controller will allow each UAV to converge to the peak of its respective potential function. Advantages of this method are that the same extremum controller parameters do not change and that the UAVs will always converge to the specified point regardless of starting position. The drawback of this method is that it involves a less decentralized approach since the user must specify the points to which the UAVs will be guided. Convergence for single node artificial potential guidance is defined when [9]

$$\dot{\psi}_{Ex} = \dot{\psi}_{ss} + \varepsilon$$
(4.5)

where $\dot{\psi}_{Ex}$ is the extremum controller heading rate command, $\dot{\psi}_{ss}$ is the desired steady-state heading rate, and ε is a margin chosen to determine convergence.

The ideal location of the artificial potential function is on the line connecting the two ground antennas. A best guess at the location of the optimal loitering position can be made using the line-of-sight SNR model. **Error! Reference source not found.** shows the combined potential for UAV1 with links to ground node 1 and UAV 2. Figure 20 shows the SNR cost function along the straight line path between ground node 1 and UAV 2, assuming the second UAV 2 is stationary and located at x=1000 m.

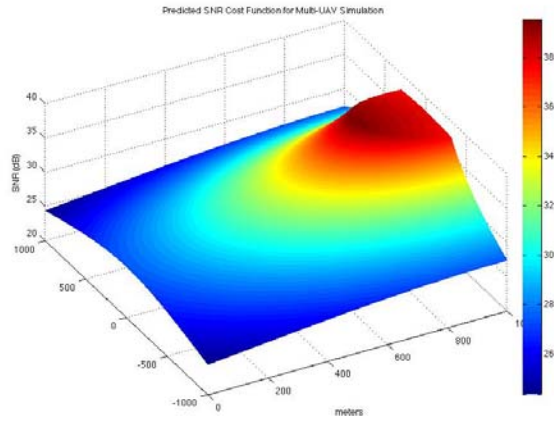


Figure 20. SNR Map for UAV1 with Links to Ground Node 1 and UAV 2

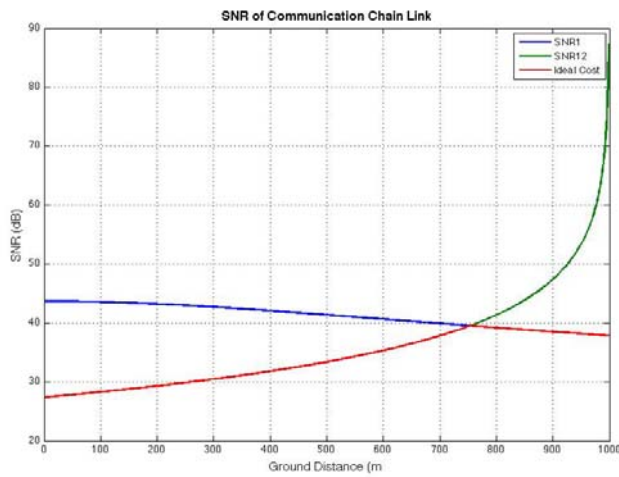


Figure 21. SNR Potential Function Along Straight Path Between Nodes

The ideal cost plot shows the combined potential function along this path has a maximum when both SNR_1 and SNR_{12} are equal. The point where this maximum occurs is the predicted optimal loitering location where an artificial potential function should be placed for initial guidance. In an actual flight experiment, once the UAVs have converged to the artificial peaks, guidance will be shifted to decentralized extremum control to guide the UAVs to the actual optimal loitering location.

D. DECENTRALIZED EXTRUMUM CONTROL FOR TWO UAVS

1. Convergence Control

For convergence during distributed extremum control mode the following criteria must be met for convergence [1].

$$\begin{aligned} \Delta J_{UAV1} &= |J_1 - J_{12}| < 1 \\ \text{and} \quad \Delta J_{UAV2} &= |J_2 - J_{12}| < 1 \end{aligned} \tag{4.6}$$

After these conditions are met the UAV positions will be near optimal and the control mode will switch to formation control.

E. LOITERING FORMATION CONTROL

Once the optimal point for communication relay has been reached, the UAVs fly in a coordinated formation that minimizes the SNR oscillations of the communication link between the UAVs. The final loitering path will be a circular orbit over the optimal point with the 2 UAVs flying in a synchronized pattern

1. Optimal Loitering Formation

The predicted SNR value of the link between the UAVs is determined by two variables: the separation distance between the aircraft and the difference in the roll angle between the two aircraft. The goal for an optimal loitering formation is to maintain a constant separation distance and maintain a constant roll angle. To achieve this result, the UAVs should fly an orbit in the same direction with their orbits synchronized in phase.

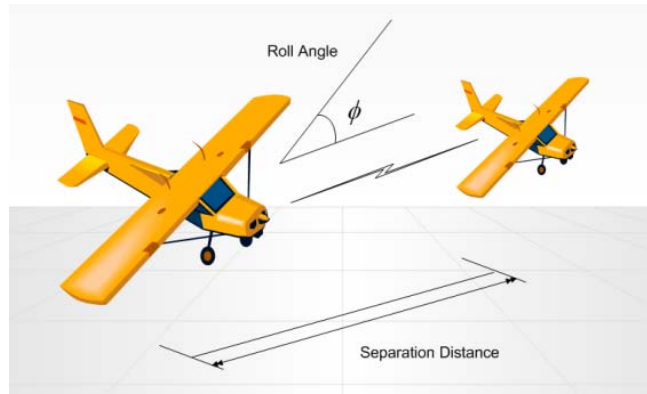


Figure 22. Formation Synchronization Parameters

To confirm that this case provides optimal link quality, four different synchronization patterns were simulated. Each case tested different synchronized phase spacing for orbits in the same direction. In the four simulations the follower aircraft synchronized its orbit in-phase, 90° ahead, 90° behind, and 180° out of phase with the lead aircraft.

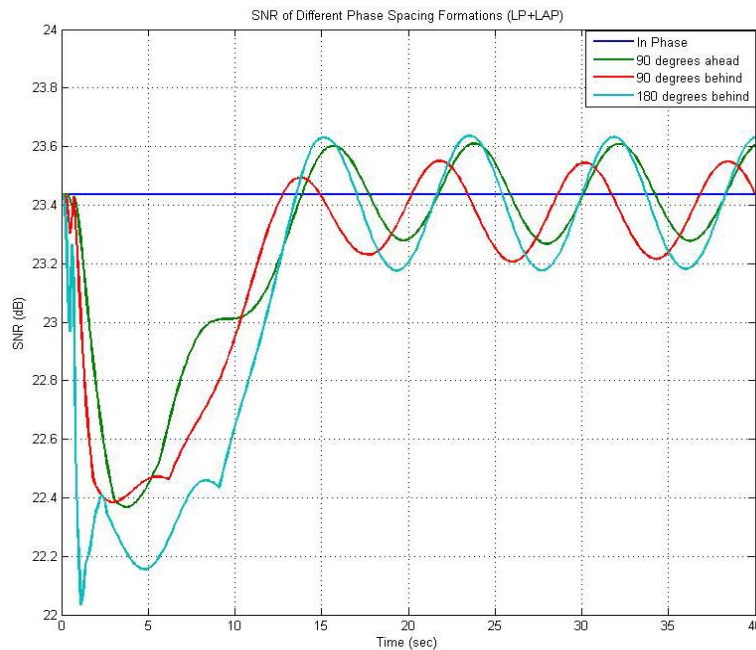


Figure 23. SNR of Phase Spacing Configurations for Loitering Formation

These simulations show that in-phase motion of an orbit in the same direction provides the greatest stability with small variations in SNR.

2. Synchronization Method 1 – Logic Controller

The first method developed to guide the UAVs to a synchronized formation was using a logic controller that adjusts the circular orbit size for each aircraft. The coordinated logic controller used in this simulation was developed with Stateflow, a state machine compatible with Simulink. With block diagrams, Stateflow executes logic in real-time and allows the programmer to observe when the system shifts from one state to the next. The logic-controller synchronizes the phasing of the UAVs by commanding one aircraft to fly a larger or smaller orbit that will result in in-phase motion.

Once the control is switched to loitering mode, one UAV is considered the leader and the other the follower. The lead aircraft continues to fly at a fixed radius above its optimal loitering position. The logic controller commands the follower aircraft to fly a circular orbit that will synchronize its orbit with that of the leader. To take into account uncertainty, the follower recalculates a new compensating loop every time its heading crosses 0 degrees. Once the follower has completed the loop it will arrive at 0 degrees approximately the same time as the leader. Shown below is a flight path of the follower aircraft in loitering mode.

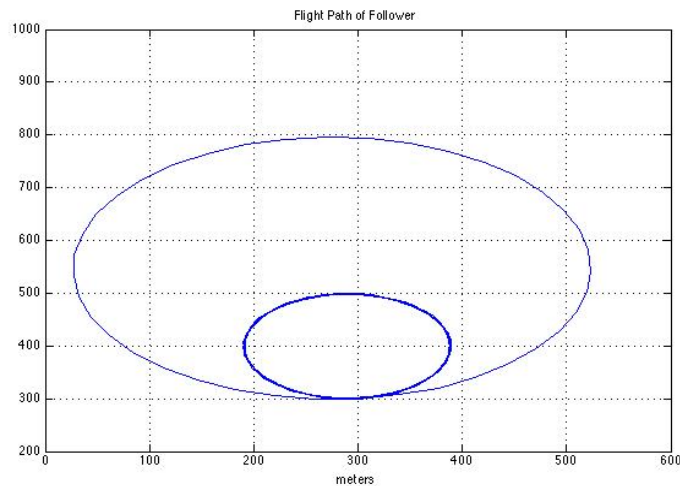


Figure 24. Synchronization Flight Path of Follower Aircraft

Once a desired loitering radius is picked, the steady state heading rate command is given to the lead aircraft.

$$\dot{\psi} = \frac{V_{com}}{r_0} \quad (4.7)$$

where V_{com} is the commanded forward velocity and r_0 is the desired loitering radius.

When the follower UAV crosses zero degrees, the heading difference between the UAVs is determined and used to calculate the new constant radius that the follower must fly to synchronize with the leader. Adding the heading difference to the desired steady state circumference determines the circumference of the new circle that the follower must fly.

$$s_{new} = 2\pi r_0 + r_0 \cdot \Delta\psi = 2\pi r_{new} \quad (4.8)$$

$$\text{for } \psi_1 = 0, \quad \begin{cases} \Delta\psi = -\psi_2 & \text{if } \psi_2 \leq \pi \\ \Delta\psi = 2\pi - \psi_2 & \text{if } \psi_2 > \pi \end{cases} \quad (4.9)$$

If UAV 1 is behind the leader it will fly a smaller circle to catch up to UAV 2. If it is ahead, UAV 1 will fly a larger circle to allow UAV 2 to catch up.

$$r_{new} = r_0 + \frac{r_0 \cdot \Delta\psi}{2\pi} \quad (4.10)$$

$$\dot{\psi}_{new} = \frac{V}{r_{new}} = \frac{V}{\left(r_0 + \frac{r_0 \cdot \Delta\psi}{2\pi}\right)} \quad (4.11)$$

The advantages of using this logic controller are fast convergence to a synchronized formation and little drifting from the desired loitering location. The drawbacks are that the controller is not robust to external disturbances and requires an accurate vehicle model. For distributed formation keeping, it is more desirable to use feedback to account for modeling discrepancies.

3. Synchronization Method 2 – Phase Controller

An alternate method of synchronizing the UAV orbits is through a feedback phase controller. Using a method derived from a Kuramoto model for synchronizing harmonic oscillators, the phase error for the two UAV formation is defined as [6]

$$\dot{\psi}_{cmd,UAV2} = \dot{\psi}_{ss} + K \sin(\psi_1 - \psi_2) \quad (4.12)$$

where K is a feedback gain from a classical PID controller. The feedback controller drives the phase error to zero and results in a synchronized formation with both UAVs flying at heading rate of $\dot{\psi}_{ss}$. However, using only phase error for feedback control results in a final loitering orbit offset from the optimal loitering location. To correct for this position shift a second feedback controller is used to drive the center of the current orbit to the location of the optimal loitering point.

Once UAVs converge on their respective loitering points and shift from gradient ascent to loiter mode, the optimal position is calculated for each UAV by finding the center of the orbit.

$$\begin{aligned} X_{center} &= X_{UAV} + \left(\frac{V}{\dot{\psi}_{ss}} \right) \cos(\psi) \\ Y_{center} &= Y_{UAV} - \left(\frac{V}{\dot{\psi}_{ss}} \right) \sin(\psi) \end{aligned} \quad (4.13)$$

The center of the current orbit is calculated using position, heading, and heading rate measurements.

$$\begin{aligned} X_{center} &= X_{UAV} + \left(\frac{V}{\dot{\psi}_{UAV}} \right) \cos(\psi) \\ Y_{center} &= Y_{UAV} - \left(\frac{V}{\dot{\psi}_{UAV}} \right) \sin(\psi) \end{aligned} \quad (4.14)$$

The distance between the current orbit center and the desired orbit center gives the offset error, \tilde{r} , which is input into a PID controller.

$$\tilde{r} = \|X_{center,UAV} - X_{center}\| \quad (4.15)$$

$$\dot{\psi}_{cmd,UAV2} = \dot{\psi}_{ss} + K \cdot \tilde{r} \quad (4.16)$$

Combining these two controllers gives the desired heading command

$$\dot{\psi}_{cmd,UAV2} = \dot{\psi}_{ss} + w_1 \cdot K_1 \sin(\psi_1 - \psi_2) + w_2 \cdot K_2 \cdot \tilde{r} \quad (4.17)$$

where w_1 and w_2 are weighting factors such that

$$w_1 + w_2 = 1 \quad (4.18)$$

This controller simultaneously synchronizes the follower aircraft with the leader while maintaining an orbit over the optimal relay point.

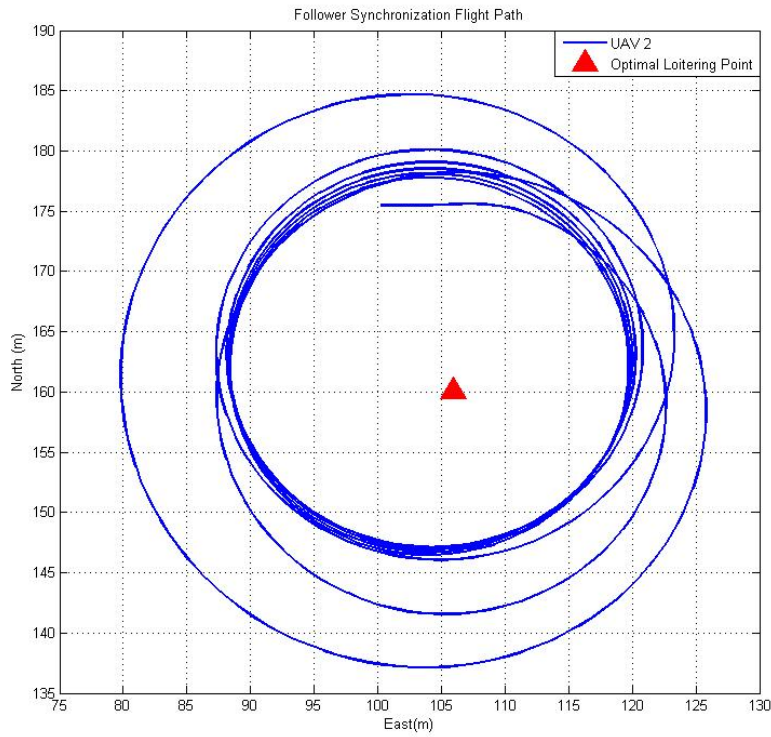


Figure 25. Follower Flight Path with Phase Feedback Control

F. MULTIPLE UAV SIMULATION

The following simulation combines the decentralized control techniques described above to guide two UAVs to the optimal relay locations to form a communication chain. This simulation has three modes shown in the flow chart below.

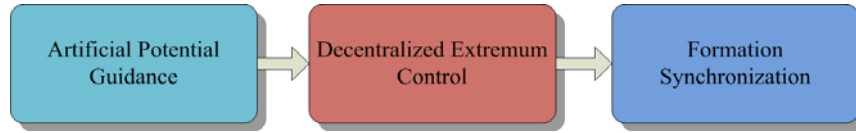


Figure 26. Control Mode Flowchart

Initial guidance is provided via the virtual node method and a phase feedback controller synchronizes the UAVs at the final stage.

Table 1. Simulation Parameters

Position Ground Tower 1 (East, North, Up)	(0, 0, 5) m
Position Ground Tower 2 (East, North, Up)	(-1972,2356,5) m
Ground Antenna Gain	14 dB
UAV Antenna Gain	6 dB
Transmitter Power	28 dBm
Noise Level	-95 dB
Frequency	2400 MHz

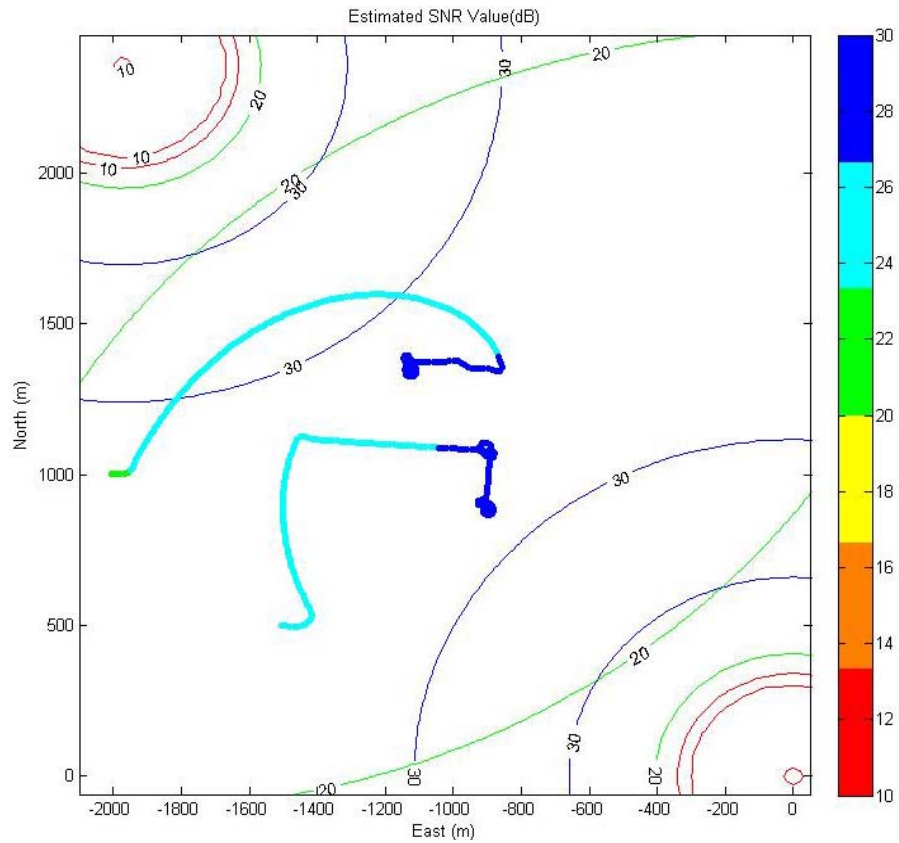


Figure 27. Multiple UAV Simulated Flight Trajectory with SNR Estimates

This simulation shows the simulated UAVs converging at the optimal communication relay points and synchronizing their orbits. The final loitering locations are at points nearly on the line connecting the two ground towers, which provides near optimal SNR values for all links in the communication chain.

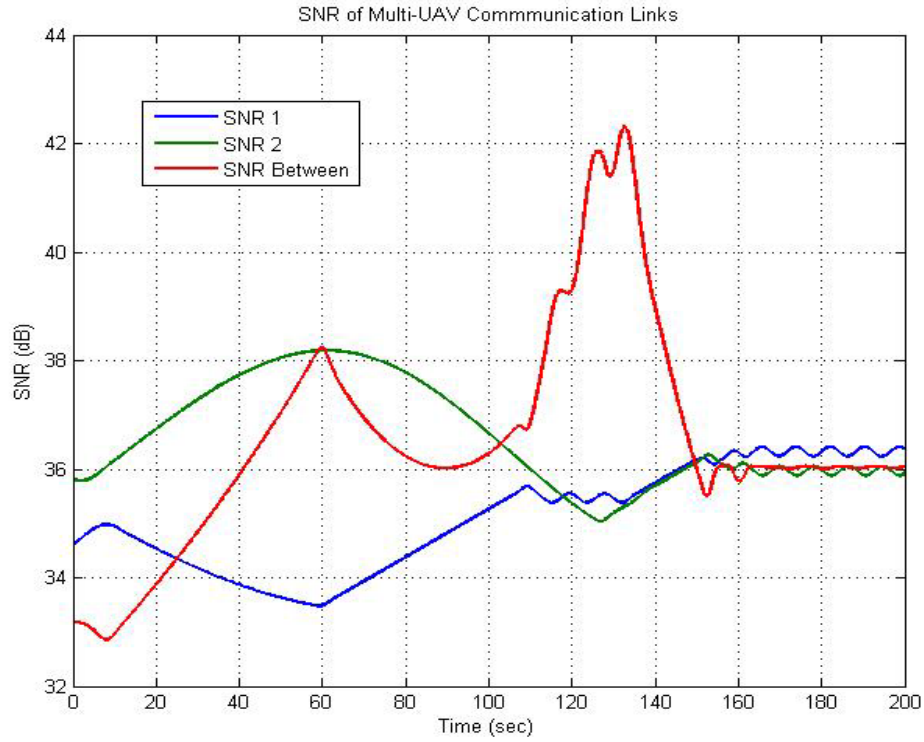


Figure 28. SNR Values for Multiple UAV Simulation

The plot of SNR shows that the SNR values of links are driven to the same optimal value just above 36 dB. The synchronization at the final stage eliminates SNR oscillations in the link between the UAVs.

V. FUTURE APPLICATIONS

A. MULTIPLE UAV RELAY TO MULTIPLE NODES

It has already been demonstrated that UAV relay nodes can be used to optimize the coverage of a network for multiple ground users spread out over a large area. To improve network coverage, multiple UAVs can be used cooperatively as relay nodes. Using multiple UAVs cooperatively allows the relay nodes to adapt to the positions of the ground users more quickly and extend the range of a network. In the simulated case, four ground nodes were spaced out in a square pattern and two UAVs were used to optimize SNR across the network. Each UAV was linked to two of the ground nodes and the other UAV. The distributed cost function of each UAV in this case becomes

$$\begin{aligned} J_{UAV1} &= \min(J_1, J_2, J_{between}) & J_{UAV2} &= \min(J_3, J_4, J_{between}) \\ &= \kappa \left(\frac{1}{J_1} + \frac{1}{J_2} + \frac{1}{J_{between}} \right) & &= \kappa \left(\frac{1}{J_3} + \frac{1}{J_4} + \frac{1}{J_{between}} \right) \end{aligned} \quad (5.1)$$

where $J_1, J_2, J_3,$ and J_4 are the SNR values of the link with each ground node and $J_{between}$ is the SNR value of the link between the UAVs. The UAVs were initially placed in the close to the middle of the square tower pattern and are guided their respective optimal loitering locations. Once converged, the UAVs synchronize their orbits using the phase feedback controller previously described.

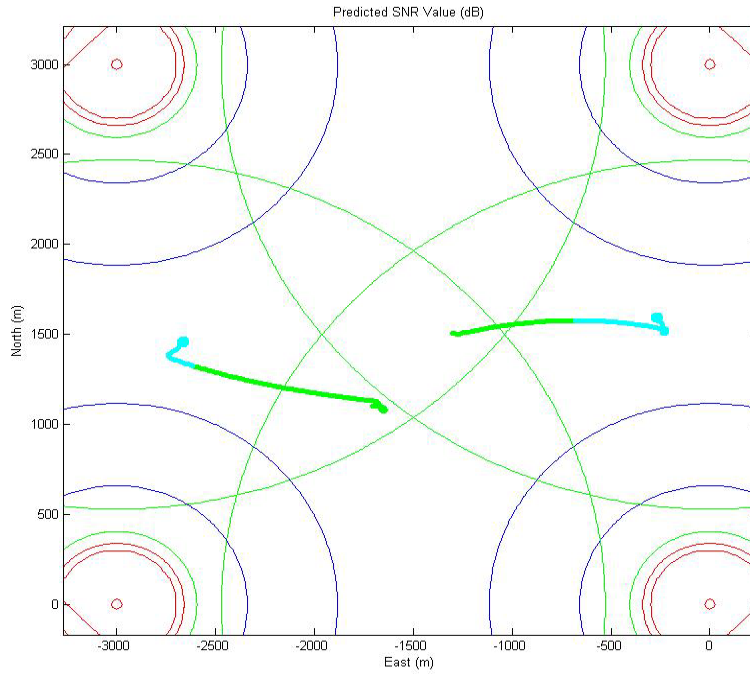


Figure 29. Vehicle Trajectory for 2 UAV and 4 Ground Node Simulation

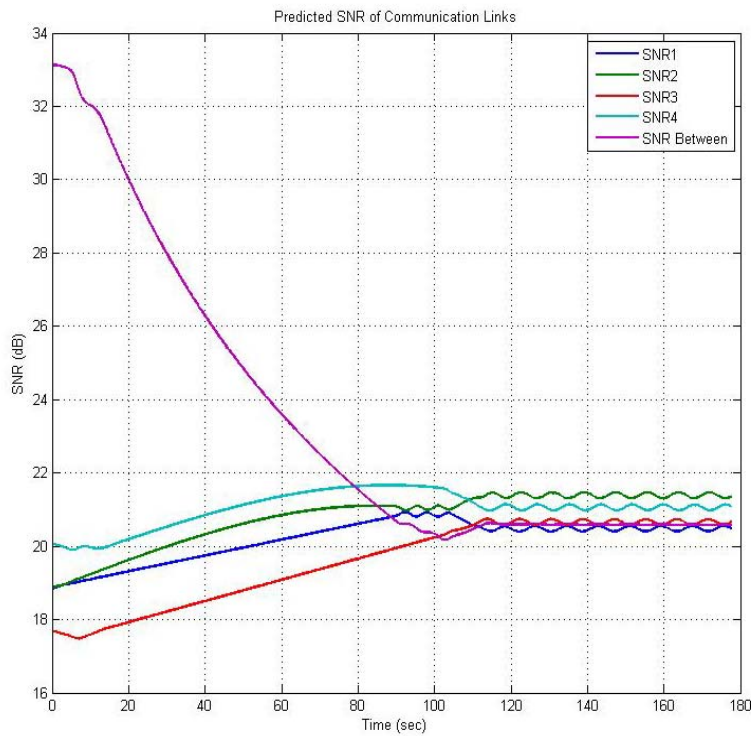


Figure 30. SNR Values for 2 UAV and 4 Ground Node Simulation

In this simulation, the final SNR value was a lower value than in the previous cases due to the larger separation distance between nodes.

B. TARGET TRACKING AND SURVEILLANCE

In addition to optimizing a mesh network, self-tuning extremum control can also be used for target tracking and surveillance applications. The goal of using an extremum controller, as opposed to a waypoint or path following controller, is to provide a distributed navigation scheme. Designating several targets as artificial potential functions modeled as ground antennas, a single UAV can navigate to a target, conduct surveillance, and continue to the next target. Using only extremum control causes the UAV to fly a path that overshoots the target, which would be undesirable for navigation. To correct for this overshoot, a Line-of-sight controller can be combined with the extremum controller. The LOS control can come from a vision based navigation system or coordinates designated by a ground station. Assuming the coordinates of the target are known, the desired heading angle, ψ_d , can be calculated using the vehicles current position. In the simulated scenario, a single UAV is commanded to track a series of targets, which in this case are modeled as ground antennas from the previous simulations. The UAV is guided to each target with a combined line-of-sight and extremum controller, loiters above the target, and continues on to the next target.

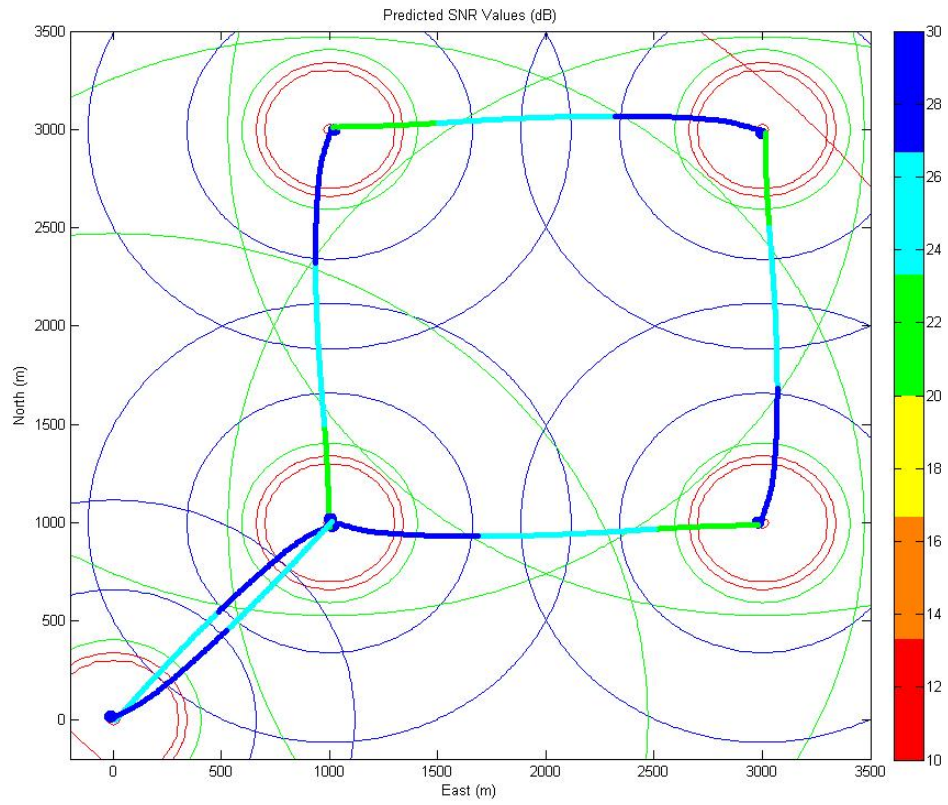


Figure 31. Vehicle Trajectory for Extremum Target Tracking Simulation

VI. CONCLUSIONS AND FUTURE WORK

A. CONCLUSIONS

This thesis extended previously developed self-tuning extremum control techniques developed for communication relay to be used with multiple relay nodes in a distributed wireless sensor network. Simulations confirmed the feasibility of implementing this scenario in real time and achieving optimal results. Additionally decentralized control techniques were applied to scenarios involving network coverage control, target tracking and surveillance.

B. FUTURE WORK

Future work in using decentralized extremum control will focus on experimental implementation of the developed control algorithms. The simulations created in this thesis will be verified with a flight test at a future date using two UAVs and two ground nodes to form a communication chain. Research is currently being conducted at NPS to explore the possibility of using soaring gliders to extend the endurance of a mission. These gliders could potentially be used as relay nodes with an extremum controller and optimize communication over a wireless sensor network for a longer time periods.



Figure 32. NPS Soaring Glider. From [2].

THIS PAGE INTENTIONALLY LEFT BLANK

APPENDIX: SIMULINK DIAGRAMS

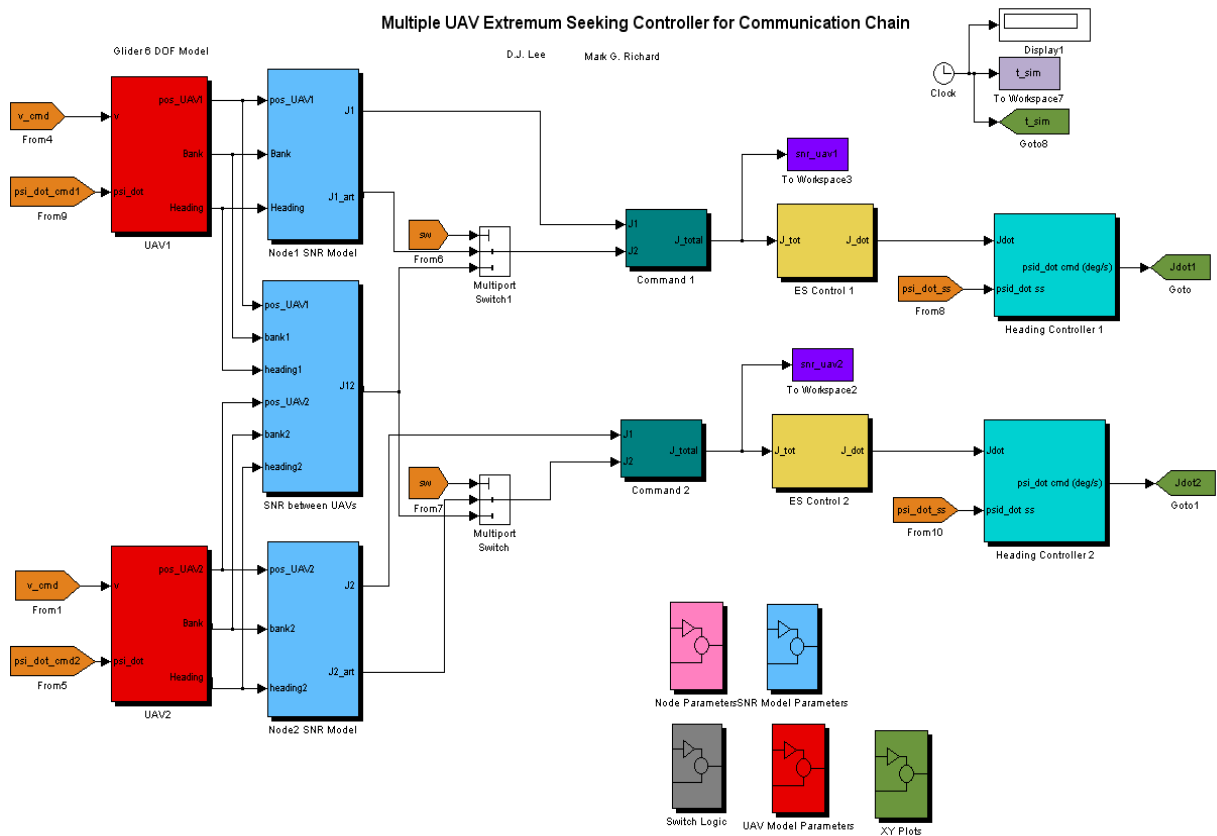


Figure 33. Multiple UAV Simulation Block Diagram

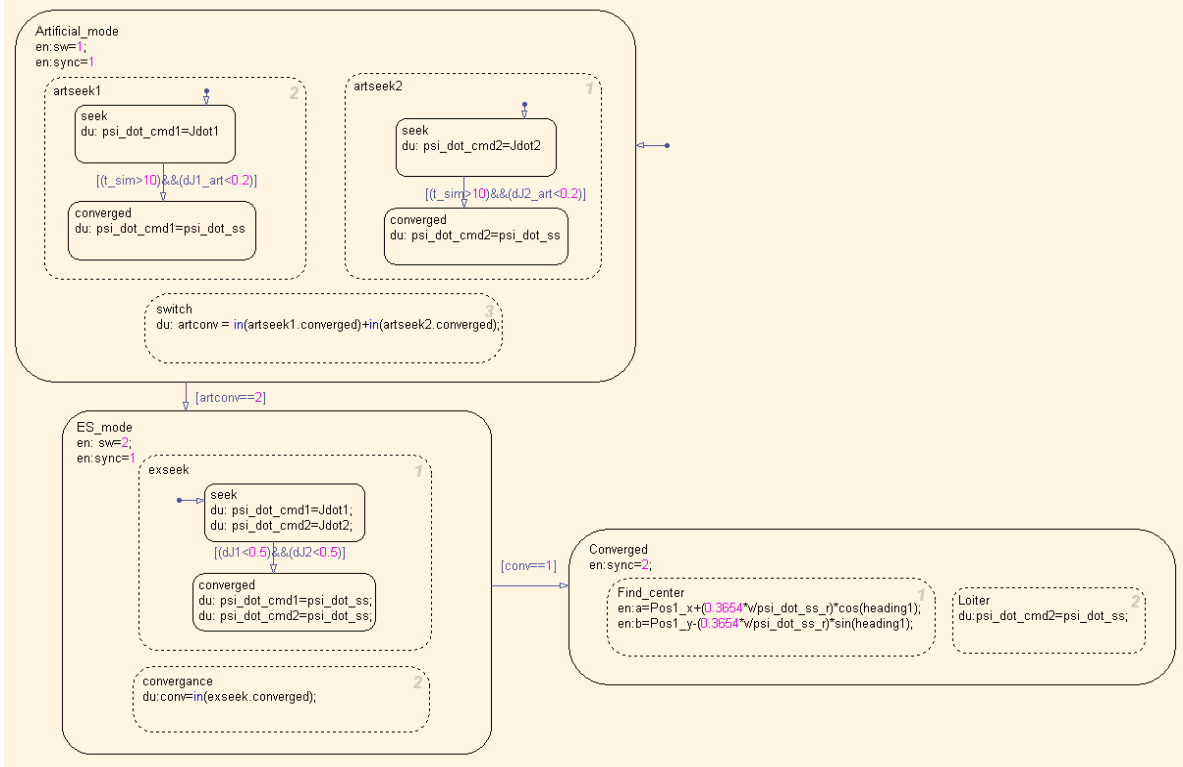


Figure 34. Stateflow Control Mode Switching Logic

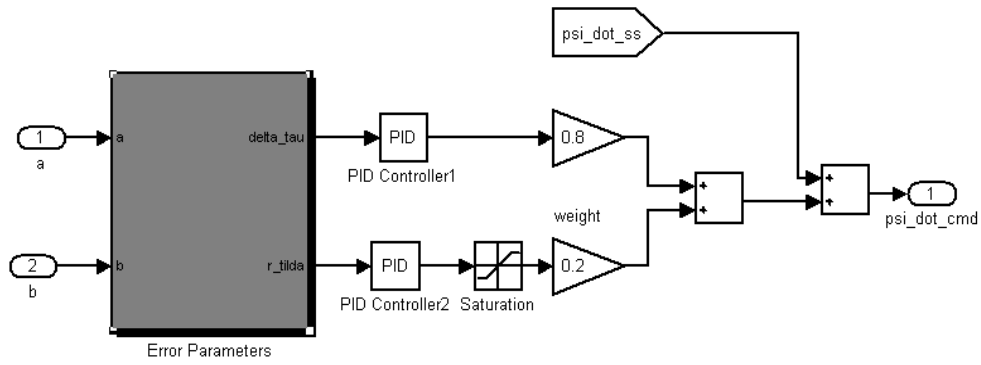


Figure 35. Phase Synchronization Controller

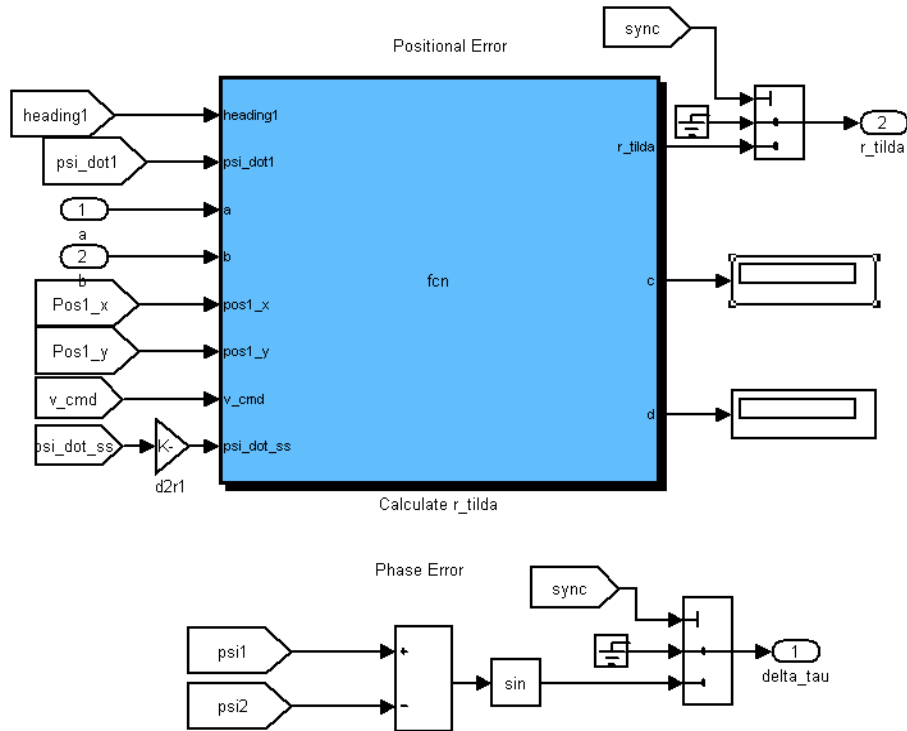


Figure 36. Phase Synchronization Phase and Orbit Center Error Calculations

A. ORBIT CENTER ERROR CALCULATION SCRIPT

```
function[r_tilda,c,d]=
fcn(heading1,psi_dot1,a,b,pos1_x,pos1_y,v_cmd,psi_dot_ss)
% calculate radial distance of current orbit center to desired orbit
center
% Using center point of orbit, heading is CW/0 North
c=pos1_x+(0.3654*v_cmd/psi_dot1)*cos(heading1);
d=pos1_y-(0.3654*v_cmd/psi_dot1)*sin(heading1);
r_tilda=sqrt((c-a)^2+(d-b)^2);
end
```

THIS PAGE INTENTIONALLY LEFT BLANK

LIST OF REFERENCES

- [1] D. J. Lee, K. Kam, I. Kaminer, S. P. Kragelund, D. P. Horner, K. Andersson, and K. Jones. "Wireless Communication Networks Between Distributed Autonomous Systems Using Self-Tuning Extremum Control," in *AIAA Unmanned Unlimited Conference*, 2009, pp. 1-22.
- [2] K. Kam. "High Bandwidth Communication Links Between Heterogeneous Autonomous Vehicles Using Sensor Network Modeling and Extremum Control Approaches," M.S. thesis, Naval Postgraduate School, Monterey, CA, 2008.
- [3] D. J. Lee, "Decentralized Control of Distributed Autonomous Systems Using Gradient Estimator Based Extremum Control" Final Report, Center for Autonomous Vehicle Research, Naval Postgraduate School, June 2009.
- [4] M. Krstic, *Real-time Optimization by Extremum Seeking Control*. John Wiley & Sons, 2003.
- [5] C. Dixon and E. Frew. "Decentralized Extremum-Seeking Control of Nonhomologic Vehicles to Form a Communication Chain." In *Proceedings of 7th International Conference on Cooperative Control and Optimization*, Gainesville, FL, January 2007, pp. 1-12.
- [6] N. Leonard. "Oscillator Models and Collective Motion: Spatial Patterns in the Dynamics of Engineered and Biological Networks," *IEEE Control Systems Magazine*, Vol. 27, No. 4, August 2007, pp.89-105.
- [7] J. Cortez, S. Matinez, T. Karatas, and F. Bullo. "Coverage Control for Mobile Sensing Networks." *IEEE Transactions on Robotics and Automation*, Vol. 20, No. 2, 2004, pp. 1-13.
- [8] C. Dixon and E. Frew. "Controlling the Mobility of Network Nodes Using Decentralized Extremum Seeking," *Proceedings of the 45th IEEE Conference on Decision & Control*, 2006, pp. 1291-1296.
- [9] D. J. Lee, K Kham, I. Kaminer, S. P. Kragelund, K Andersson, and K. D. Jones. "High Bandwidth Communication Links Between Distributed Unmanned Systems for Wireless Sensor Networks Using Small UAVs via Extremum Seeking Control," Internal Report, Center for Autonomous Vehicle Research, Naval Postgraduate School, 2008, pp. 1-20.

THIS PAGE INTENTIONALLY LEFT BLANK

INITIAL DISTRIBUTION LIST

1. Defense Technical Information Center
Ft. Belvoir, Virginia
2. Dudley Knox Library
Naval Postgraduate School
Monterey, California
3. Professor Isaac I. Kaminer
Naval Postgraduate School
Monterey, California
4. Dr. Deok Jin Lee
Naval Postgraduate School
Monterey, California
5. Professor Knox T. Millsaps
Chairman, Department of Mechanical and Astronautical
Naval Postgraduate School
Monterey, California